Metallomics

Accepted Manuscript

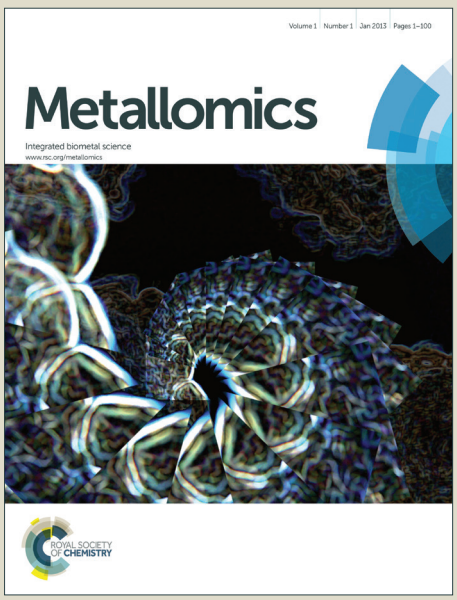

ROYAL SOCIETY OF CHEMISTRY

www.rsc.org/metallomics

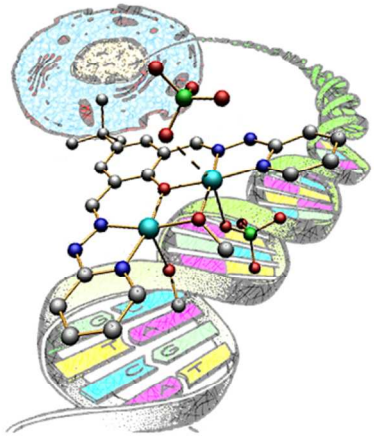

Metallomics

RSCPublishing

ARTICLE

Highly Cytotoxic DNA-Interacting Copper(II) Coordination Compounds

Cite this: DOI: 10.1039/x0xx00000x

Received 00th January 2014,
Accepted 00th January 2014

DOI: 10.1039/x0xx00000x

www.rsc.org/

Rosa F. Brissos,[a] Ester Torrents,[a] Francyelli Mariana dos Santos Mello,[b] Wanessa Carvalho Pires,[b] Elisângela de Paula Silveira-Lacerda,[b]* Ana B. Caballero,[a] Amparo Caubet,[a] Chiara Massera,[c] Olivier Roubeau,[d] Simon J. Teat,[e] and Patrick Gamez*[af]

Four new Schiff-base ligands have been designed and prepared by condensation reaction between hydrazine derivatives (*i.e.* 2-hydrazinopyridine or 2-hydrazinoquinoline) and mono- or dialdehyde (respectively 3-*tert*-butyl-2-hydroxybenzaldehyde and 5-*tert*-butyl-2-hydroxyisophthalaldehyde). Six copper(II) coordination compounds of various nuclearities have been obtained from these ligands, which are formulated as [Cu(**L1**)Cl](CH$_3$OH) (**1**), [Cu(**L2**)NO$_3$] (**2**), [Cu$_2$(**L3**)(ClO$_4$)$_2$(CH$_3$O)(CH$_3$OH)](CH$_3$OH) (**3**), [Cu$_2$(**L4**)(ClO$_4$)(OH)(CH$_3$OH)](ClO$_4$) (**4**), [Cu$_8$(**L3**)$_4$(NO$_3$)$_4$(OH)$_5$](NO$_3$)$_3$(CH$_3$OH)$_5$(H$_2$O)$_8$ (**5**) and [Cu$_3$(**HL2'**)$_4$Cl$_6$](CH$_3$OH)$_6$ (**6**), as revealed by single-crystal X-ray studies. Their DNA-interacting abilities have been investigated using different characterization techniques, which suggest that the metal complexes act as efficient DNA binders. Moreover, cytotoxicity assays with several cancer cell lines show that some of them are very active, as evidenced by the sub-micromolar IC$_{50}$ values achieved in some cases.

Introduction

Chemotherapy is almost exclusively based on organic compounds and natural products. Though, metal complexes have received a great deal of attention as potential chemotherapeutic agents in the past three decades.[1-5] Actually, the discovery of the antiproliferative properties of *cis*-diamminedichloroplatinum(II) (cisplatin) in the late 1960's[6, 7] initiated the interest for metal-based anticancer drugs. Cisplatin has shown remarkable activities against a variety of solid tumours, with for instance a survival rate of over 90% in the case of testicular cancer.[8] However, cisplatin treatment is limited by a number of drawbacks. Indeed, cisplatin may cause serious side effects such as nephrotoxicity, emetogenesis or neurotoxicity.[8-10] Additionally, drug resistance, both inherited and acquired, may be faced with cisplatin, which is moreover not orally bioavailable.[11] Consequently, tremendous research efforts have been devoted to the development of new anti-tumour active coordination compounds with improved pharmacological properties.[12]

Copper is an essential trace element in the human body (*i.e.* copper is an important biometal[13]) where it is involved in a variety of vital oxidation-reduction (redox) processes.[14-16] Nevertheless, any alteration of its normal metabolism will convert it into a toxic agent.[17, 18] Actually, the potential toxicity of this redox metal arises from its ability to generate Reactive-Oxygen Species (ROS) that will cause oxidative damage to biomolecules such as lipids, proteins, DNA and RNA.[19, 20] In fact, elevated concentrations of copper have been observed in several cancer cell lines, including brain, lung, colon, breast and prostate.[21] Hence, a conceivable strategy for the development of new cancer chemotherapies is to generate complexes of biometals (such as copper) that will eradicate malignant cells without being rapidly and massively excreted by the human body (in contrast to cisplatin). As a matter of fact, investigations carried out in this area of bio-inorganic chemistry have generated a number of biologically active complexes with interesting carcinostatic properties.[22-27]

Since the past seven years, we have been involved in the design of readily-available ligands for the preparation of copper(II) (and zinc(II)) coordination compounds with interesting DNA-interacting properties.[28-33] In that context, a square-planar copper(II) complex with remarkable DNA-cleaving properties was obtained from a very simple Schiff-base ligand, namely 4-methyl-2-*N*-(2-pyridylmethylene)aminophenol (Hpyrimol; Scheme 1).[33] In addition, the use of Hpyrimol allowed the synthesis of efficient nuclease-active zinc(II) complexes, whose DNA-cleaving activities were based on the ligand, through the generation of phenoxyl radicals.[31, 34]

In the present study, we took inspiration from Hpyrimol to design and prepare a series of easily accessible ligands (*i.e.* obtained through one reaction step from readily available reactants) containing the three coordinating moieties found in the original ligand, *viz.* a phenol group, an imine function and a pyridine unit (Scheme 1).

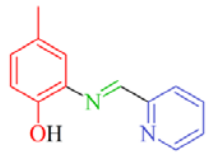

Scheme 1. Ligand 4-methyl-2-*N*-(2-pyridylmethylene)aminophenol (Hpyrimol).[33, 35] The three coordinating groups are shown in distinct colours, *i.e.* the phenol in red, the imine in green and the pyridine in blue.

Thus, four ligands have been synthesized (Scheme 2) and six copper(II) coordination compounds have been obtained with different metal salts. The complexes have been fully characterized and their potential interactions with DNA have been investigated thoroughly using various techniques. *In vitro* cytotoxicity assays have shown that most of the complexes prepared exhibit highly efficient cytotoxic behaviours against several cancer cell lines, as illustrated by the very low IC_{50} values achieved in some cases, which are significantly lower than the corresponding ones obtained with cisplatin.

Results and Discussion

Ligand synthesis: Our ligand design combines the three coordinating groups (shown in distinct colours; Scheme 2) found in the ligand Hpyrimol (Scheme 1). The N,N,O ligands are easily synthesized in good yields (66−91%), by means of a Schiff-base condensation reaction between a hydrazinopyridine derivative and a phenolcarboxaldehyde. Hence, the ligand 2-*tert*-butyl-6-(pyridine-2-ylhydrazonomethyl)phenol (**HL1**; Scheme 2) was obtained by reaction of 2-hydrazinopyridine with 3-*tert*-butyl-2-hydroxybenzaldehyde. The bulky *tert*-butyl substituent was purposely chosen as a potential stabilizer of a phenoxyl radical species;[36] indeed, with the ligand Hpyrimol, the formation of phenoxyl radicals has been clearly observed,[34] which allowed to explain the DNA-cleaving abilities of zinc/pyrimol complexes.[31] For the ligand 2-*tert*-butyl-6-(quinoline-2-ylhydrazonomethyl)phenol (**HL2**; Scheme 2), the pyridine unit has been replaced by a quinoline group with the objective to increase the DNA-intercalating properties[37-39] of the resultant metal complexes. The ligands 4-*tert*-butyl-2,6-bis-(pyridine-2-ylhydrazonomethyl)phenol (**HL3**; Scheme 2) and 4-*tert*-butyl-2,6-bis-(quinoline-2-ylhydrazonomethyl)phenol (**HL4**; Scheme 2) are the dinucleating versions (the phenol group potentially acting as a bridging ligand) of respectively **HL1** and **HL2**. These N,N,O,N,N ligands are prepared by reaction of the hydrazine derivatives used to synthesize **HL1** and **HL2** with a bis-carboxaldehyde phenol, namely 5-*tert*-butyl-2-hydroxyisophthalaldehyde. Again, a bulky, electron-donating *tert*-butyl group has been included on the phenolic ring to stabilize the phenoxyl radical that may be produced upon coordination to the metal ion.

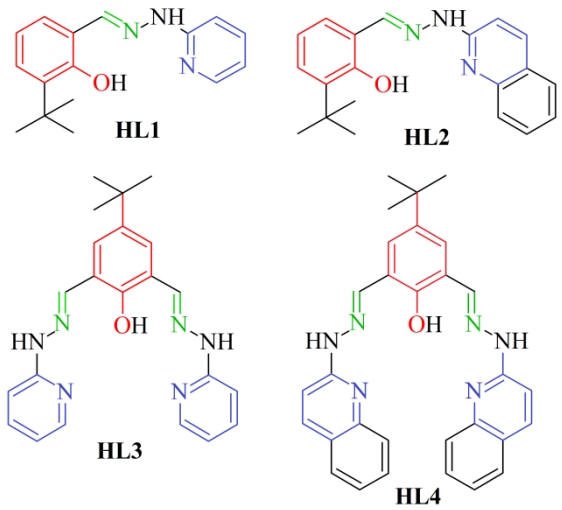

Scheme 2. Representations of the mononucleating ligands 2-*tert*-butyl-6-(pyridine-2-ylhydrazonomethyl)phenol (**HL1**) and 2-*tert*-butyl-6-(quinoline-2-ylhydrazonomethyl)phenol (**HL2**), and the dinucleating ligands 4-*tert*-butyl-2,6-bis-(pyridine-2-ylhydrazonomethyl)phenol (**HL3**) and 4-*tert*-butyl-2,6-bis-(quinoline-2-ylhydrazonomethyl)phenol (**HL4**). The three different types of coordinating groups, *i.e.* the phenol, the imine and the pyridine, are shown in distinct colours.

Complexes containing two metal ions bridged by the phenolic group are expected with the ligands **HL3** and **HL4**. In fact, such phenol-bridged dinuclear copper(II) compounds are commonly used to mimic the active site of type-3 copper enzymes and their oxidative properties.[40, 41] Therefore, these ligands have been designed with the intention of increasing the DNA-oxidative-cleaving capabilities of the corresponding copper systems.

Complex synthesis and structure: Reaction of one equivalent of **HL1** with one equivalent of copper(II) chloride dihydrate in methanol produces the coordination compound [Cu(**L1**)Cl]CH_3OH (**1**), whose molecular structure, determined by single-crystal X-ray diffraction, is depicted in Figure 1. Crystallographic and refinement parameters are summarized in Table S1, and selected coordination bond lengths and angles are listed in Table S3.

The copper centre in **1** exhibits the expected square-planar geometry, which is comparable to that observed for the complex [Cu(pyrimol)Cl].[33, 42] Actually, the Cu−O, Cu−N and Cu−Cl bond lengths varying from 1.877(2) to 2.254(1) Å are closely related to those of the pyrimol complex, so are the coordination angles in the range 80.93(9)−97.38(6)° (Table S3).[33] Moreover, the crystal packing of **1** is similar to that of [Cu(pyrimol)Cl], the copper complexes being associated by means of π−π interactions (Figure S1 and Table S3).

Reaction of one equivalent of **HL2** with one equivalent of copper(II) nitrate trihydrate in methanol yields the pseudo square-planar coordination compound [Cu(**L2**)NO_3] (**2**). A representation of the molecular structure of **2** determined by single-crystal X-ray diffraction is shown in Figure 2.

Crystallographic and refinement parameters are summarized in Table S1, and selected coordination bond lengths and angles are listed in Table S3.

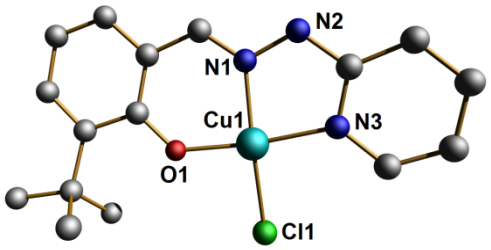

Fig. 1. Representation of the molecular structure of **1** with partial atom-numbering scheme. The hydrogen atoms and the lattice methanol molecule are not shown for clarity.

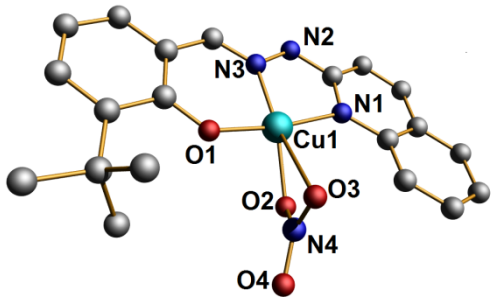

Fig. 2. Representation of the molecular structure of **2** with partial atom-numbering scheme. The hydrogen atoms are not shown for clarity.

The coordination geometry about the copper ion is almost a square plane. Indeed, the metal centre is coordinated by the N,N,O ligand and a nitrate oxygen atom (O2) with normal Cu−N and Cu−O bond lengths of respectively 1.924(2)−2.008(2) Å and 1.883(2)−1.964(2) Å. Additionally, Cu1 is semi-coordinated by a second oxygen atom (O3) of the bidentate nitrate anion, at a long distance of 2.878(2) Å (Table S3). The coordination angles (within the square plane) in the range 87.90(8)−99.93(9)º are comparable to those of [Cu(pyrimol)Cl].[33] Again, the mononuclear molecules are associated by means of π−π interactions (Figure S2 and Table S3), like for **1** and [Cu(pyrimol)Cl].

Reaction of one equivalent of the dinucleating ligand **HL3** with two equivalents of copper(II) perchlorate hexahydrate in methanol generates the dicopper complex $[Cu_2(\mathbf{L3})(ClO_4)_2(CH_3O)(CH_3OH)](CH_3OH)$ (**3**). A representation of the molecular structure of **3**, determined by single-crystal X-ray diffraction, is depicted in Figure 3. Crystallographic and refinement parameters are summarized in Table S1, and selected coordination bond lengths and angles are listed in Table S4.

Compound **3** exhibits two copper(II) ions with distinct coordination geometries. Cu1 is in a pseudo-octahedral environment formed by the ligand donor atoms N1, N3 and O1 in the equatorial plane, which is completed by a methoxide oxygen atom (O3S). The axial positions are occupied by two perchlorate anions; one of them is coordinated at a distance of 2.612(7) Å (O7), while the other is semi-coordinated, as illustrated by the Cu1−O2 bond length of 2.913(8) Å (Table S4).

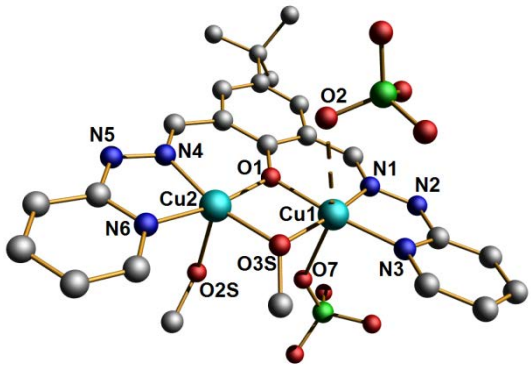

Fig. 3. Representation of the molecular structure of **3** with partial atom-numbering scheme. The hydrogen atoms and the lattice methanol molecule are not shown for clarity.

The equatorial angles varying from 80.2(2) to 106.6(2)º reveal a strong distortion of the octahedron, which is most likely due to the phenoxide and methoxide bridges, and to the small bite angle N−Cu−N imposed by the anionic ligand **L3**. Cu1 is bridged to Cu2 through the phenoxide unit of **L3** (oxygen atom O1) and a methoxide ligand (O3S). Actually, O1 and O3S form part of the basal plane of the square-pyramidal geometry observed for Cu2, which is completed by the ligand nitrogen atoms N4 and N6. The Cu−O and Cu−N bond distances are in normal ranges. The axial position is occupied by a methanol molecule (O2S), at a normal Cu−O distance (Table S4). The tau-factor amounts to 0.05 for Cu2, which characterizes a square-pyramidal coordination environment.[43] Actually, the basal angles vary from 80.8(2) to 105.7(2)º (the values are comparable to those found in the equatorial plane of Cu1; see above), the deviations from the ideal angle of 90º again originating from the two bridges (O1 and O3S), and the small N−Cu−N bite angle of **L3**. The Cu1 and Cu2 ions are separated by a short distance of 2.943(2) Å. In the crystal packing, the molecules of **3** are interacting *via* an intricate network of hydrogen bonds involving the lattice and coordinated solvents molecules (O2S and O3S), and the amine functions N2 and N5 (Table S4).

Reaction of one equivalent of the dinucleating ligand **HL4** with two equivalents of copper(II) perchlorate hexahydrate in methanol produces the dicopper compound $[Cu_2(\mathbf{L4})(ClO_4)(OH)(CH_3OH)](ClO_4)$ (**4**). A representation of the molecular structure of **4**, determined by single-crystal X-ray diffraction, is shown in Figure 4. Crystallographic and refinement parameters are summarized in Table S2, and selected coordination bond lengths and angles are listed in Table S4.

The structure of **4** is somehow related to that of **3**. Indeed, **4** also exhibits two copper(II) centres with different coordination geometries. Cu1 is pentacoordinated and its square-pyramidal environment (tau = 0.10) is formed by the nitrogen atoms N1 and N3 and the oxygen atom O1 belonging to the anionic ligand **L4**, the hydroxide oxygen atom O2 and the perchlorate

oxygen atom O5. The donors N1, N3, O1 and O2 constitute the basal plane of the square pyramid whose apical position is occupied by O5.

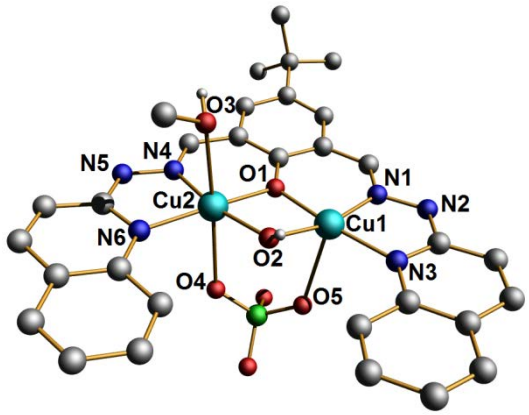

Fig. 4. Representation of the molecular structure of **4** with partial atom-numbering scheme. The hydrogen atoms (except the two OH hydrogens; oxygen atoms O2 and O3) and the lattice perchlorate anion are not shown for clarity.

The bond distances and angles are comparable to those observed for Cu2 in **3** (see Table S4). Cu1 is triply bridged to Cu2 that exhibits an octahedral geometry. The equatorial plane of the octahedron is constituted of the atoms N4, N6 and O1 from the ligand **L4**, and the bridging hydroxide atom O2. The axial positions are occupied by a methanol molecule (O3) and the oxygen atom O4 from the perchlorate anion that bridges Cu2 to Cu1 (in addition to the phenoxide and hydroxide bridges). The Cu−N and Cu−O are in normal ranges, and are comparable to those of Cu1 in **3**. The equatorial angles vary from 79.28(17) to 108.8(2)º, thus indicating a strong distortion of the octahedron, as noticed for Cu1 in **3**. The copper(II) ions are separated by a distance of 2.981(2) Å. Finally, in contrast to **3**, the crystal packing of **4** reveals the occurrence of π−π interactions between the dinuclear molecules, which give rise to the formation of a 1D supramolecular chain (Figure S3 and Table S4). This feature supports our ligand design with the use of a quinoline group to favour π interactions (compared to the pyridine-containing ligands).

Reaction of one equivalent of **HL3** with two equivalents of copper(II) nitrate trihydrate in methanol yields the unexpected octanuclear coordination compound $[Cu_8(\mathbf{L3})_4(NO_3)_4(OH)_5](NO_3)_3(CH_3OH)_5(H_2O)_8$ (**5**). A representation of the molecular structure of **5**, determined by single-crystal X-ray diffraction, and an illustration of its bis-open-cubane core are shown in Figures 5A and 5B, respectively. Crystallographic and refinement parameters are summarized in Table S2, and selected coordination bond lengths and angles are listed in Table S5.

The solid-state structure of **5** can be regarded as the assembly of four dinuclear $[Cu_2(\mathbf{L3})]$ units (each of these units resembling compound **3**; see Figure 3) that are bridged by hydroxide ligands. This association gives rise to the formation of two open-cubane-like structures that are connected by a single hydroxide bridge (oxygen atom O1E), generating the octanuclear complex **5** (Figure 5B). This cluster compound is formed by six octahedral copper(II) ions (Cu1B, Cu1C, Cu1D, Cu2A, Cu2B and Cu1D) and two square-pyramidal copper(II) ions (Cu1A and Cu2C). The equatorial plane of all octahedra contains a deprotonated ligand **L3** (N, N, O donors) and a bridging hydroxide anion. The metal centres differ by the axial ligands. The axial positions are occupied by a monodentate nitrate anion and a bridging hydroxide for Cu1B and Cu1D. Cu1C and Cu2A are coordinated by a bridging nitrate anion (connecting the metal ions to Cu2C and Cu1A, respectively) and a bridging hydroxide. Finally, in the case of Cu2B and Cu2D, the axial positions are occupied by two bridging hydroxide anions. The basal plane of the pentacoordinated Cu1A and Cu2C cations is constituted of a deprotonated ligand **L3** and a hydroxide anion. The apical position of the square pyramid (tau = 0.00 for Cu2C and tau = 0.01 for Cu1A) is occupied by a bridging nitrate anion (connecting the metal ions to Cu2A and Cu1C, respectively). All Cu−N and Cu−O bond lengths (Table S5) can be regarded as normal for the four different coordination environments observed in **5**. The equatorial (octahedral geometry) and basal (square-pyramidal geometry) angles are very similar to those observed for complexes **3** and **4** (see Tables S4 and S5).

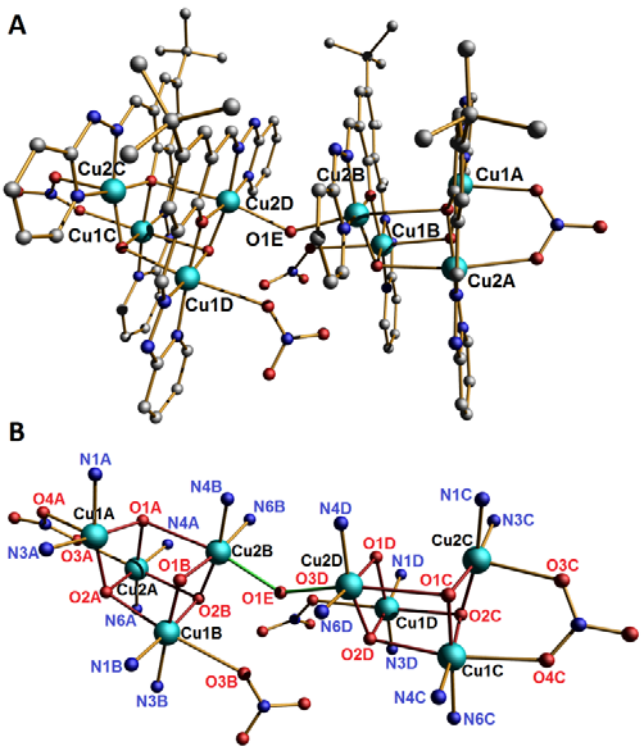

Fig. 5. A) Representation of the molecular structure of **5** with partial atom-numbering scheme. The hydrogen atoms and the lattice nitrate anions, methanol and water molecules are not shown for clarity. B) Octanuclear core with atom-numbering scheme.

The Cu···Cu separation distances within the octanuclear complex vary from 2.869(4) to 4.342(2) Å. Actually, the longest distance corresponds to Cu2B···Cu2D, which are the metal centres through which the two cubane units are connected

via the hydroxide bridge O1E. Lastly, an intricate network of strong hydrogen bonds (Table S5), involving the lattice nitrate anions and methanol and water molecules, is observed in the solid-state structure of **5**.

Reaction of 1.33 equivalents of **HL2** with one equivalent of copper(II) chloride dihydrate produces the trinuclear compound $[Cu_3(\mathbf{HL2'})_4Cl_6](CH_3OH)_6$ (**6**), whose solid-state structure obtained by single-crystal X-ray diffraction reveals that the original ligand **HL2** has suffered a cyclization reaction generating the 1,2,4-triazolo[4,3,a]quinoline derivative **HL2'** (see Figure 6). Crystallographic and refinement parameters are summarized in Table S2, and selected coordination bond lengths and angles are given in Table S6.

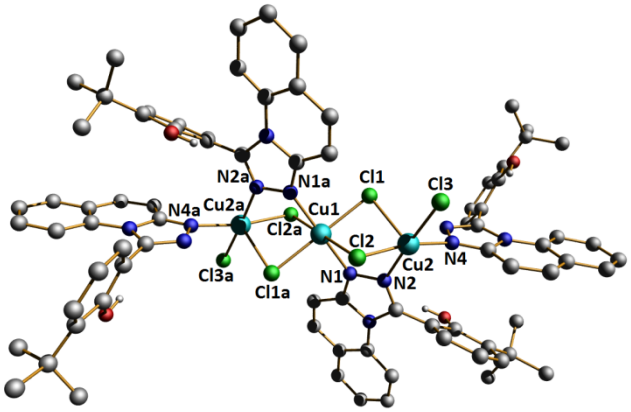

Fig. 6. Representation of the molecular structure of **6** with partial atom-numbering scheme. Only the phenolic hydrogen atoms are shown and the lattice methanol molecules are omitted for clarity. Symmetry operation: a = 1−x, 1−y, 1−z.

The trinuclear core of compound **6** is formed by a central octahedral copper(II) ion, *i.e.* Cu1, that is bridged to the two symmetry-related external copper(II) ions Cu2 and Cu2a, which exhibit a square-pyramidal geometry. The equatorial plane of Cu1 contains the nitrogen atoms N1 and N1a from two ligands **HL2'** and the chloride atoms Cl1 and Cl1a. The axial positions are occupied by the chloride atoms Cl2 and Cl2a. The Cu−N and Cu−Cl bond lengths are in normal ranges for this type of chromophore, and the equatorial coordination angles varying from 89.37(10) to 90.63(10)º are indicative of an almost perfect octahedral geometry (Table S6). Cu2 (and Cu2a; symmetry operation: a = 1−x, 1−y, 1−z) is in a square-pyramidal environment (tau = 0.12), whose basal plane is constituted of two nitrogen atoms, namely N2 and N4 belonging to two different **HL2'** ligands, and two chlorides, *i.e.* Cl2 and Cl3. The apical position is occupied by the chloride anion Cl1. The Cu−N and Cu−Cl bond distances and the angles can be regarded as normal for this type of coordination environment (Table S6). Cu2 and Cu2a are triply connected to the central Cu1 ion, by means of two chloride bridges and one N,N-bridging triazolo ligand **HL2'**, giving rise to a Cu···Cu separation distance of 3.292(1) Å. In the crystal packing of **6**, the neutral complex is interacting with the lattice methanol molecules *via* hydrogen bonds with coordinated chlorides and the phenolic hydrogen atoms. In addition, the trinuclear units are involved in π−stacking interactions (see Table S6) through two of their fused heteroaromatic rings, generating a 1D supramolecular chain (Figure S4).

It should be mentioned here that the preparation of 1,2,4-triazolo[4,3,a]pyridine and 1,2,4-triazolo[4,3,a]quinoline derivatives by oxidative cyclization of hydrazones (of the type of ligand **HL2**), is typically carried out with iodobenzene diacetate (*i.e.* $PhI(OAc)_2$) as the oxidant,[44, 45] but other oxidants can be used as well.[46-48] In the present case, copper(II) ions most likely act as an oxidation agent to generate **HL2'**. Actually, the generation of such 1,2,4-triazolo compounds by cyclization reaction of hydrazones in the presence of atmospheric dioxygen and catalytic amounts of copper dichloride has been described in the literature.[49]

After having fully characterized the different complexes prepared, the consequent step has been to study their potential interaction with DNA using different techniques.

UV-Vis spectroscopy: this technique is commonly used to study potential interactions (and their likely nature) between DNA and metal complexes.[50] Hence, the potential binding of complexes **1**–**6** to calf thymus DNA (ct-DNA) was investigated using UV-Vis spectroscopy. To this aim, absorption spectra at a constant complex concentration, *i.e.* 25 μM, in the absence and presence of increasing amounts of ct-DNA (namely 0–50 μM) have been recorded. Figure 7 shows the corresponding spectra for **1**, which are representative of the other compounds examined in the present study (namely complexes **2**–**6**; see Figure S5).

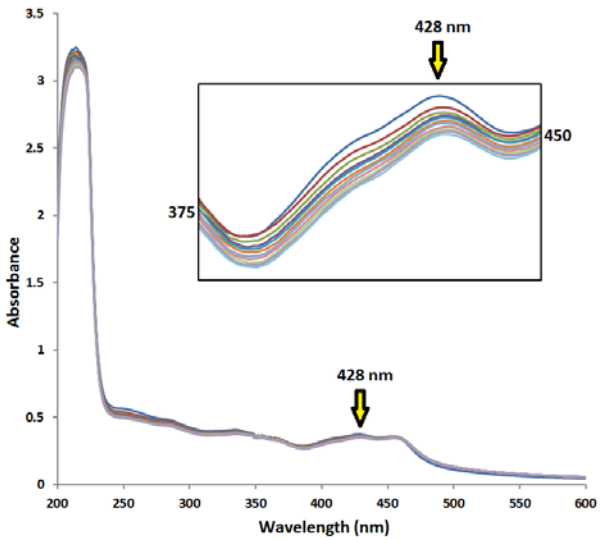

Fig. 7. Absorption spectra of complex **1** in Tris-HCl buffer (pH = 7.2) upon addition of ct-DNA. The insert shows an enlargement of the region 375–450 nm where the metal-to-ligand charge-transfer (MLCT) absorption is located. Concentration of complex: 25 μM; [ct-DNA]: 0 –25 μM (the concentration of ct-DNA was determined from its absorption intensity at 260 nm with a molar extinction coefficient of 6600 M^{-1} cm^{-1}).

Specific bands observed in the region 250–300 nm that are assigned to π–π* transitions of the ligands, and around 350–450 nm, which are attributed to metal-to-ligand charge-transfer

(MLCT) absorptions, were used to analyze the respective binding affinities of the metal compounds. The spectroscopic data for all complexes reveal a hypochromic effect without red shift (Figures 7 and S5), which suggest that the compounds most likely bind to DNA by means of electrostatic interactions or groove binding[51, 52](while a red shift of the absorptions associated to hypochromism would have indicated interaction through ligand intercalation[53-55]). Thus, **1**–**6** appear to bind to DNA via groove mode.[56]

To compare quantitatively the binding affinities of compounds **1**–**6** to ct-DNA, the intrinsic binding constants K_b were determined using equation (1)

$$\frac{[DNA]}{\varepsilon_a - \varepsilon_f} = \frac{[DNA]}{\varepsilon_0 - \varepsilon_f} + \frac{1}{Kb\,(\varepsilon_0 - \varepsilon_f)} \quad (1)$$

where [DNA] is the concentration of DNA in base pairs, ε_a the extinction coefficient observed at the given DNA concentration, ε_f the extinction coefficient of the free complex in solution (A_{obs} / [complex]), and ε_0 the extinction coefficient of the complex when fully bound to DNA.

A plot of [DNA] / (ε_a – ε_f) *versus* [DNA] gives a slope corresponding to 1 / (ε_a – ε_f) and a y-intercept equal to 1 / K_b (ε_a – ε_f), respectively. Thus, the intrinsic binding constant K_b is the ratio of the slope to the intercept. The [DNA] / (ε_a – ε_f) *vs.* [DNA] plots obtained for **1**–**6** are depicted in Figure 8. The binding constants range from 0.80 to 3.41 10^5 M^{-1} (Table 1), therefore revealing strong DNA-binding affinities of the copper compounds. The complexes can be classified into two groups. Indeed, compounds **1**, **4** and **6** exhibit high binding strengths (with K_b values of respectively 2.67 10^5 M^{-1}, 3.41 10^5 M^{-1} and 2.93 10^5 M^{-1}; Table 1), while **2**, **3** and **5** are comparatively less efficient (K_b values in the range 0.80–1.31 10^5 M^{-1}; Table 1). It can be noticed that complex **6**, whose molecular structure is distinct (compared to those of **1**–**5**, as the result of the modification of the original ligand in **6**; see above), shows a relatively strong binding affinity for ct-DNA (K_b = 2.93 10^5 M^{-1}; Table 1), which is comparable to those of **1** and **4**.

Table 1 Intrinsic binding constants K_b determined for complexes **1**–**6**.[a]

Complex	Slope ($\times 10^{-3}$)	Intercept ($\times 10^{-9}$)	K_b[b] (10^5 M^{-1})	Log K_b
1	1.75	6.55	2.67 ± 0.15	5.43
2	0.36	2.75	1.31 ± 0.11	5.12
3	0.24	3.00	0.80 ± 0.01	4.91
4	0.76	2.23	3.41 ± 0.13	5.53
5	0.04	0.35	1.26 ± 0.09	5.10
6	0.15	0.53	2.93 ± 0.12	5.47

[a] Linear [DNA] / (ε_a – ε_f) *vs.* [DNA] plots are obtained for [complex]:[DNA] ratio ≤ 1:1; [b] K_b is obtained from the ratio of the slope to the intercept. The K_b errors have been determined from the measurement in quadruplicate for each complex.

The observed K_b constants, in the order of 10^5 M^{-1}, point to a possible groove binding of the copper compounds to the ct-DNA duplex. Actually, the binding constants of the efficient major-groove binder methyl green (Scheme 3) is in the order of 10^6 M^{-1},[57] and those of the minor groove binders Hoechst 33258 and DAPI (Scheme 3) are in the order of 10^8 M^{-1},[58, 59] and 10^6 M^{-1}, respectively.[60] These DNA-interacting molecules are aromatic cations that exhibit planar structures (Scheme 3).

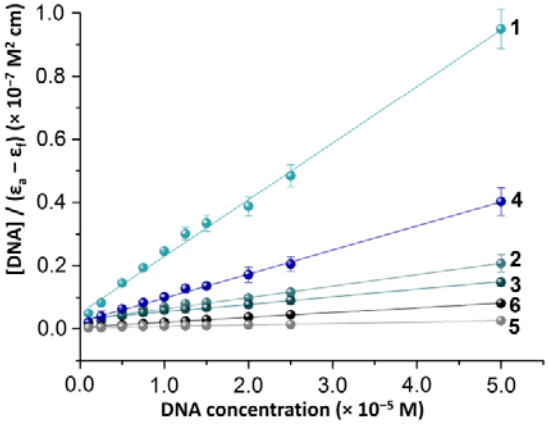

Fig. 8. Plots of [DNA] / (ε_a – ε_f) *vs.* [DNA] for the titration of ct-DNA with complexes **1**–**6** at 428 nm (yellow arrow in Figure 7): experimental data points and linear fitting of the data. Concentration of complex: 25 μM; [DNA]: 0 –50 μM. For complex **5**, a concentration of 10 μM was used.

It should be noted that the cationic parts of the complexes described herein (namely after removal of the labile chloride, nitrate or perchlorate anions and also of the coordinated solvent molecules) are planar as well and may therefore act as minor- or/and major-groove binders (depending on their size and/or shape).

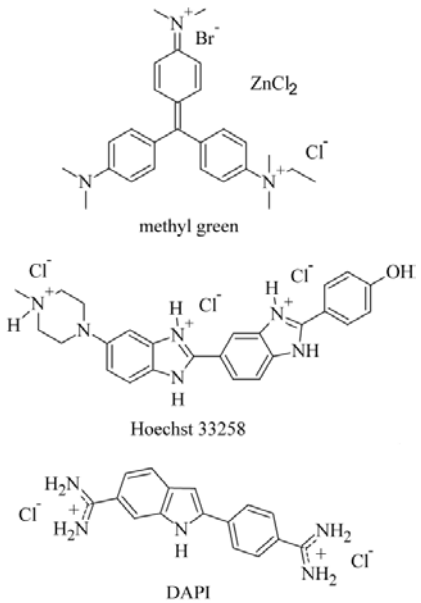

Scheme 3. Schematic representations of the structures of the planar groove binders 4-{[4-(dimethylamino)phenyl][4-(dimethyliminiumyl)cyclohexa-2,5-dien-1-ylidene]methyl}-N-ethyl-N,N-dimethylanilinium bromide chloride, zinc chloride salt (methyl green), 2′-(4-hydroxyphenyl)-5-(4-methyl-1-piperazinyl)-2,5′-bi-1H-benzimidazole trihydrochloride (Hoechst 33258) and 4′,6-diamino-2-phenylindole dihydrochloride (DAPI).

ESI-MS and EPR spectroscopy: electrospray-ionization mass-spectrometry (ESI-MS; positive mode) measurements have been carried out (see Figures S6–S12), which reveal that

planar cationic moieties indeed are present in solution for compounds **1**, **3** and **4** (see Figures S6, S8 and S9, respectively), under the experimental conditions used (for instance, the samples have been dissolved in DMSO prior to their introduction into the spectrometer). Compounds **2** and **6** do not appear to be stable under the mass-spectrometry conditions applied (which are different to those used for the spectroscopic investigations). A nitrate-bridged dicopper species (containing a planar **L2**/Cu unit as in **2**) is observed for **2** (Figure S7), while trinuclear **6** is clearly unstable since free ligand **HL2'** is detected (Figure S12). Though, a bulky (**HL2'**)$_2$/Cu complex, which obviously originates from the external copper centres of **6**, is found (Figure S12). It should be noted here that the copper species arising from complexes **2** and **6** can function as DNA binders as well. In the case of **5**, as might be expected, the hydroxy-bridged bis-cubane unit is not observed; however, cubane moieties (obtained by cleavage of the hydroxide bridge Cu2B–O1E–Cu2D; Figure 5) are detected (Figures S10 and S11).

Since most studies have been performed in Tris-HCl buffer, the potential ability of this buffer to bind copper(II) ions has been examined by EPR spectroscopy. For this purpose, copper(II) chloride was dissolved in two different solvent mixtures, namely Tris-HCl 3/DMSO 1 and Tris-HCl 1/DMSO 1. The use of DMSO was necessary since the copper complexes were not soluble in pure buffer. The corresponding frozen-solution EPR spectra are depicted in Figure S13. As evidenced in Figures S13a and S13c, Tris-HCl binds to copper(II) ions, generating an EPR spectrum with a high $g_{//}$ value and a low $A_{//}$ value, which are characteristic of copper(II) complexes in a tetrahedral geometry (it should be mentioned here that the EPR spectrum of $CuCl_2$ in pure Tris-HCl is identical).[61] Next, the frozen-solution spectra of the mononuclear complexes **1** and **2** dissolved in Tris-HCl/DMSO solvent mixtures (1-to-1 for **1** and 3-to-1 for **2**) were recorded (Figures S13b and S13d, respectively. **1** displays a rhombic spectrum with g_1, g_2 and g_3 values that are in agreement with a square-planar geometry (Figure S13b).[62] The frozen-solution EPR spectrum of **2** is silent, therefore suggesting the interaction of copper(II) ions in solution. Actually, these data corroborate those obtained by ESI-MS (see above), as dinuclear species are observed (see Figure S7), which appears to be antiferromagnetically coupled. These EPR results indicate that copper(II) ions remain bound to **L1** and **L2** (for complexes **1** and **2**, respectively) in Tris-HCl solvent mixtures, as the corresponding spectra (Figures S13b and S13d) are different than those of $CuCl_2$/(Tris-HCl/DMSO) solutions (Figures S13a and S13c).

Fluorescence spectroscopy: to investigate further the prospective character of the DNA-complex interactions occurring with the copper(II) compounds presented herein, competitive binding studies using ethidium bromide (EB) bound to ct-DNA have been carried out. EB is a DNA-intercalating agent that fluoresces when bound to the polynucleotide molecule (actually the fluorescence intensity of EB increases by almost 20-fold after binding to DNA).[63, 64] Hence, displacement of EB through the binding to DNA of a molecule will result in fluorescence quenching, therefore providing valuable information regarding the DNA affinity of the compound considered.[65, 66] It should be stated here that EB displacement by the molecule studied does not imply that it acts as an intercalator (like EB). Indeed, electrostatic interactions or groove binding may be sufficient to alter significantly the conformation of the DNA double helix, inducing the release of EB.[67, 68]

Fluorescence spectra have been recorded at constant concentrations of ct-DNA and EB, respectively 2.5 and 12.5 μM, in the presence of increasing amounts of complex, *viz.* in the range 2–150 μM. In all cases, a clear decrease in emission intensity is noticed. Figure 9 shows the corresponding spectra for **1**, which are representative of the other compounds inspected in the present study (namely complexes **2**–**6**; see Figure S14). These spectroscopic data therefore confirm the occurrence of strong interactions between the copper(II) compounds and ct-DNA, as illustrated by the release of EB.

To assess quantitatively the affinity of the different complexes for ct-DNA (compared to EB), their quenching efficiency has been evaluated using the Stern-Volmer quenching constant K_{SV}, applying equation (2)

$$\frac{I_0}{I} = 1 + K_{SV}[\text{complex}] \quad (2)$$

where I_0 and I are the emission intensities in the absence and the presence of the complex, respectively. Hence, a plot of I_0/I versus [complex] should yield a straight line with a slope equal to K_{SV}. The I_0/I versus [complex] plots obtained for **1**–**6** are depicted in Figure 10.

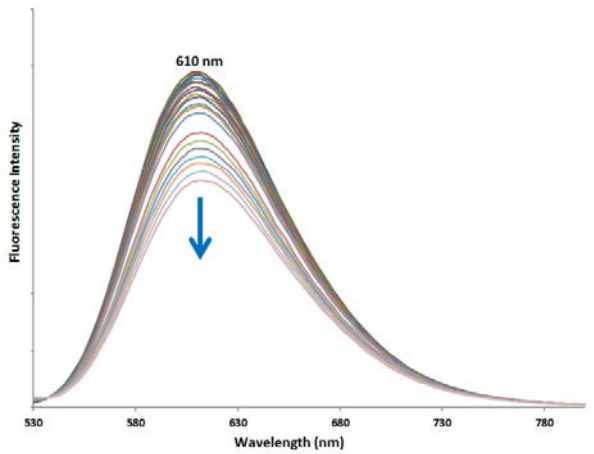

Fig. 9. Emission spectra of the DNA-EB complex (2.5 and 12.5 μM), λ_{exc} = 514 nm, λ_{em} = 610 nm, upon addition of increasing amounts of **1** (2–150 μM). The arrow shows the diminution of the emission intensity with the [**1**] increase.

The K_{SV} constants vary from 2.92 to 14.69 10^3 M^{-1} (see Table 2), revealing fairly high EB-displacing ability of all complexes. Complex **5**, *i.e.* the bis-open-cubane compound (see Figure 5), shows the highest K_{SV} value. Most likely, the interaction of this large molecule (which is expected to act as a mono-open-cubane in solution where the hydroxide bridge Cu2B–O1E–Cu2D is probably broken; in fact, mass-

spectrometry studies reveal the presence of the cubane moiety in solution while the bis-cubane is not detected – see above and Figure S12) with DNA induces a strong distortion of the biomolecule, resulting in the release of EB. This reasoning is corroborated by the K_{SV} values (Table 2) obtained for trinuclear complex **6**, which is the second bulkier compound of the series (Figure 6), and dinuclear complex **4**, whose steric hindrance comes next (Figure 4). For complexes **1**–**3**, the Stern-Volmer constants are in line with the corresponding UV-Vis spectroscopic data (see Table 1).

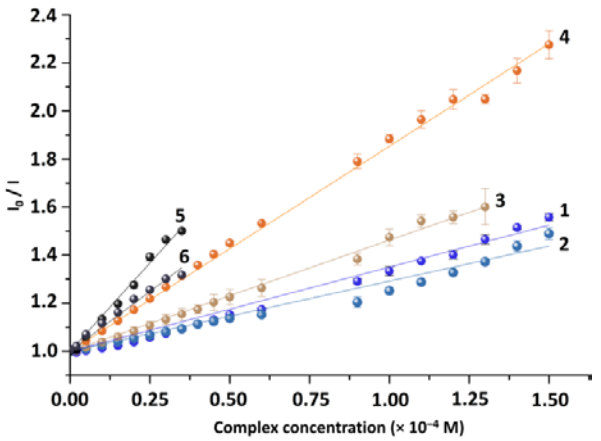

Fig. 10. Plots of I_0/I *vs.* [complex] for the titration of DNA-EB with complexes **1**–**6** at λ_{exc} = 514 nm and λ_{em} = 610 nm: experimental data points and linear fitting of the data. Concentration of complex: 2–150 μM; [DNA]: 2.5 μM; [EB]: 12.5 μM.

Table 2 Stern-Volmer constants K_{SV} determined for complexes **1**–**6** competing with EB.

Complex	K_{SV}[a] (10^3 M^{-1})	Log K_{SV}
1	3.50 ± 0.01	3.54
2	2.92 ± 0.01	3.46
3	4.62 ± 0.01	3.66
4	8.53 ± 0.01	3.93
5	14.69 ± 0.35	4.17
6	9.94 ± 0.28	4.00

[a] K_{SV} is obtained from the slope of the straight line. The K_{SV} errors have been determined from the measurement in quadruplicate for each complex.

Next, competitive binding studies have been conducted with the minor-groove binder Hoechst 33258 (Scheme 3). When bound to ct-DNA, Hoechst 33258 fluoresces at λ_{em} = 458 nm when excited at λ_{exc} = 349 nm (for free Hoechst 33258, λ_{exc} = 337 nm and λ_{em} = 508 nm).[69] As for EB (see above), its fluorescence is dramatically increased upon binding to the biomolecule, as reflected by the corresponding quantum yields of 0.015 (free dye) and 0.42 (ct-DNA–dye complex).[69] Therefore, displacement of Hoechst 33258 through the binding to DNA of a molecule will result in fluorescence quenching, which will be indicative of its tendency to interact within the minor groove of the double helix.

The K_{SV} constants vary from 2.12 to 13.51 10^4 M^{-1} (see Table 3), and are therefore an order of magnitude higher than the corresponding values obtained for EB (Table 2). These features thus suggest that compounds **1**–**6** may have a greater propensity to act as groove binders, hence corroborating the UV-Vis observations (pointing towards a non-intercalative behaviour; see above). Furthermore, the comportment of the copper complexes is radically distinct. Indeed, while the bulky compounds **5** and **6** display the highest EB-displacement properties (see above), they exhibit the poorest abilities to replace the minor-groove binder Hoechst 33258, as revealed by the low K_{SV} values of 2.12 10^4 and 3.75 10^4 M^{-1} (Table 3).

Table 3 Stern-Volmer constants K_{SV} determined for complexes **1**–**6** competing with Hoechst 33258.

Complex	K_{SV}[a] (10^4 M^{-1})	Log K_{SV}
1	4.07 ± 0.08	4.61
2	8.83 ± 0.25	4.95
3	13.51 ± 0.36	5.13
4	6.33 ± 0.16	4.80
5	3.75 ± 0.03	4.57
6	2.12 ± 0.01	4.33

[a] K_{SV} is obtained from the slope of the straight line. The K_{SV} errors have been determined from the measurement in quadruplicate for each complex.

Obviously, their great size prevents a proper interaction with the DNA minor groove; however, their likely electrostatic interactions induce the release of EB (through a non-intercalative mechanism). Compounds **1**–**4** exhibit moderate (complex **1**) to good (complex **3**) capabilities of displacing Hoechst 33258, following the sequence **3** >> **2** > **4** >> **1** (with K_{SV} values from 4.07 10^4 up to 13.51 10^4 M^{-1} (Table 3). With a K_{SV} value in the 10^{-5} M range, complex **3** appears to display the more adequate size to interact appropriately in the minor groove of DNA. As a matter of fact, **3** shows the best IC_{50} values (see Table 4); furthermore, **3** is obtained from ligand **HL3** that exhibits remarkable cytotoxic properties (especially against fibroblasts, with IC_{50} = 40 nM; see below).

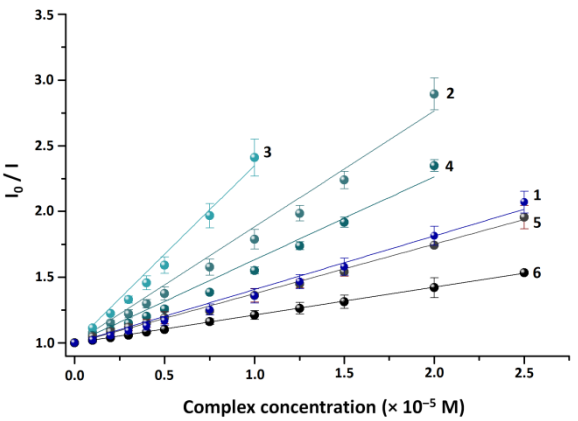

Fig. 11. Plots of I_0/I *vs.* [complex] for the titration of DNA-Hoechst 33258 with complexes **1**–**6** at λ_{exc} = 350 nm and λ_{em} = 450 nm: experimental data points and linear fitting of the data. Concentration of complex: 2–150 μM; [DNA]: 0.19 μM; [Hoechst]: 15 μM.

Gel electrophoresis: After these spectroscopic studies, the next logical step has been to observe directly the interaction of the different complexes with DNA. In that context, agarose gel electrophoresis is a common and simple method to visualize the different typical shapes of plasmid DNA, namely the normal

supercoiled form (form I), the circular nicked form (form II, which is obtained after cutting apart only one of the two strands) and the linear form (form III that is produced when both strands are broken). Hence, uncut plasmids (form I) will appear to migrate more rapidly than the same plasmid when linearized (form III). Moreover, the nicked circles (form II), which are the bulkiest, will be the slowest migrating species in the gel (since the separation is not only by charge but also by size).

As mentioned in the Introduction, the ligands **HL1**–**HL4** (Scheme 2) have been designed on the basis of the ligand Hpyrimol (Scheme 1), which allowed to generate an efficient copper-containing nuclease.[33] The potential cleaving properties of complexes **1**–**6** were therefore examined by electrophoretic mobility measurements with pBR322 plasmid DNA. A reducing agent, namely ascorbic acid, was used to induce the formation of copper(I) species, which would permit the potential formation of reactive oxygen species (ROS) that are capable of cleaving DNA. The corresponding agarose gels depicted in Figure 12 reveal a comparable behaviour for all six copper compounds.

First, it should be noted that form III (whose electrophoretic band should appear in-between those of forms I and II) is not observed. Thus, in contrast to the Cu-pyrimol complex,[33] compounds **1**–**6** are not able to linearize the plasmid DNA. This unexpected feature, especially for **1** whose crystal structure (Figure 1) closely resembles that of the square-planar Cu-pyrimol complex, may be explained by the additional nitrogen atom in the linker connecting the phenol group to the pyridine unit (see Schemes 1 and 2). This sp^3-hybridized nitrogen atom obviously disrupts the π-conjugation between the two ligand parts (contrary to the Hpyrimol ligand), which most likely gives rise to these drastically distinct properties.

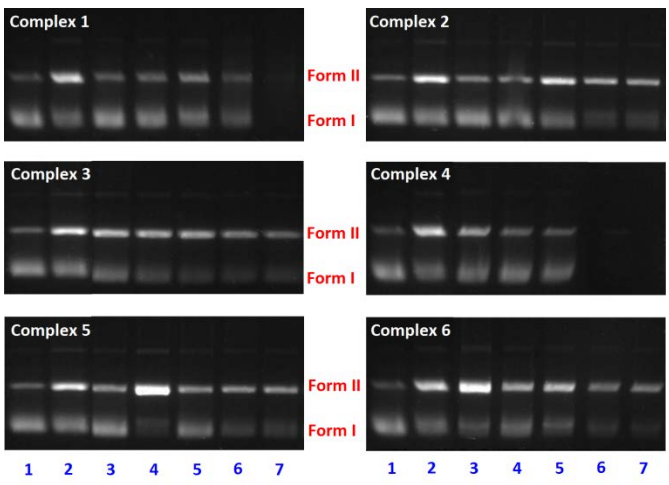

Fig. 12. Agarose gel electrophoresis images of pBR322 plasmid DNA incubated for 24 h at 37 °C with increasing concentrations of complexes **1**–**6**, in the presence of a reducing agent, *i.e.* ascorbic acid, during an additional incubation time of 1 h (lanes 3–7). Lane 1: pure plasmid DNA; lane 2: pBR322 DNA + ascorbic acid (100 μM); lane 3: [complex] = 5 μM; lane 4: [complex] = 25 μM; lane 5: [complex] = 50 μM; lane 6: [complex] = 100 μM; lane 7: [complex] = 200 μM. Each sample contains 200 ng of plasmid DNA.

Second, the intensity of the bands (for both form I and form II) decreases when the concentration of complex is increased (these bands even disappear completely for compounds **1** and **4**; Figure 12). Actually, these results suggest the occurrence of strong interactions between **1**–**6** and DNA (without cleavage of its strands), which corroborate the observations made by the previous spectroscopic measurements (see above). It appears that the complexes act as groove binders (and not as DNA cleavers), and these interactions probably produce large DNA-complex species (like for instance DNA dimers, trimers and so on, bound to metal complexes) that precipitate (hence explaining the vanishing of the electrophoretic bands when the complex concentration is raised). Finally, the peculiar features noticed for octanuclear complex **5** (lane 4 in Figure 12) and trinuclear complex **6** (lane 3 in Figure 12) may be rationalized by their more intricate structures, compared to those of **1**–**4**. Clearly, at a concentration of 25 μM for **5** and of 5 μM for **6**, form II is more abundant, therefore confirming that the structure of the DNA (form I) is affected through the binding of these compounds (as observed by fluorescence; see above). Above these concentrations, the intensity of the bands gradually diminishes when the quantities of complexes augment (as for **1**–**4**; Figure 12), thus pointing towards the formation of insoluble higher species (that are therefore not observed by gel electrophoresis).

As aforementioned, it appears that compounds **1**–**6** do not act as DNA cleavers (in contrast to [Cu(pyrimol)Cl][33]), which would involve a Cu^{II}/Cu^{I} process. Therefore, ascorbic acid most likely does not play a role in the observed interaction between the complexes and plasmid DNA. For that reason, gel-electrophoresis experiments were conducted without this reducing agent. Comparable results were obtained (see Figure S15), which corroborate the hypotheses made above.

As mentioned in the sections **UV-Vis**, **ESI-MS** and **fluorescence spectroscopies** (see above), the coordination compounds reported herein may function as minor- or/and major-groove binders. Therefore, electrophoresis studies have been carried out with the known minor-groove binder Hoechst 33258 and major-groove binder methyl green (see Scheme 3 for the structures of these two organic molecules). For this purpose, increasing amounts of the different groove binders have been incubated with pBR322 DNA at 37 ºC for 24 hours, and electrophoretized. As evidenced in Figure 13, drastically distinct behaviours are exhibited by the two DNA-interacting molecules. With the minor-groove binder Hoechst 33258 (Figure 13 top), the electrophoretic bands corresponding to DNA forms I and II gradually vanish upon increase of the concentration (corroborating the results achieved by fluorescence spectroscopy). In contrast, with the major-groove binder methyl green (Figure 13 bottom), its interaction with DNA does not seem to affect the intensity of these bands. The behaviour exhibited by Hoechst 33258 resembles that of complexes **1**–**4** (see Figure 12). These features would suggest that this copper compounds can act as DNA minor-groove binders. On the other hand, compounds **5** and **6** may interact

with the major groove of the DNA double helix (most likely as the result of their greater steric bulk).

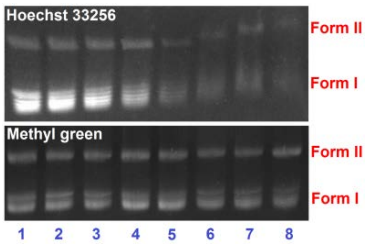

Fig. 13. Agarose gel electrophoresis images of pBR322 plasmid DNA incubated for 24 h at 37 °C with increasing concentrations of Hoechst 33258 (top) and methyl green (bottom). Hoechst 33258, lane 1: pure plasmid DNA; lane 2: [Hoechst] = 5 μM; lane 3: [Hoechst] = 10 μM; lane 4: [Hoechst] = 20 μM; lane 5: [Hoechst] = 40 μM; lane 6: [Hoechst] = 60 μM; lane 7: [Hoechst] = 80 μM; lane 8: [Hoechst] = 100 μM. Methyl green, lane 1: pure plasmid DNA; lane 2: [methyl green] = 30 μM; lane 3: [methyl green] = 60 μM; lane 4: [methyl green] = 100 μM; lane 5: [methyl green] = 150 μM; lane 6: [methyl green] = 200 μM; lane 7: [methyl green] = 300 μM; lane 8: [methyl green] = 400 μM.

AFM studies: another, less employed characterization technique to analyse the effect of a (potentially interacting) molecule on the DNA structure is atomic-force microscopy (AFM). For instance, AFM has been used successfully to observe the DNA-structural changes induced through interactions with metal complexes.[70, 71]

In the present study, pBR322 plasmid DNA (open circular was used as a starting topoisomer to allow a clear observation of any interaction of the compound investigated; indeed, any modification of this open form, namely its disappearance, will suggest a DNA/compound interaction) was incubated at 37 °C for 24 h with the different complexes ([complex] = 100 μM) in 40 mM HEPES/10 mM $MgCl_2$ buffer, as for the gel electrophoresis experiments (see Experimental Section). Actually, the AFM-sample preparation is identical to that used for the gel electrophoresis conditions of lane 6 in Figure 12, for comparison purposes. The samples were then incubated one more hour in the presence of ascorbic acid (100 μM) and subsequently imaged by AFM. As is evidenced in Figure 14, all complexes interact with DNA. Indeed, the original morphology of DNA (open circular structures; Figures 14a–b) is clearly altered after incubation with compounds **1**–**6** (Figures 14c–h), confirming the results achieved by UV-Vis, fluorescence and electrophoresis studies.

Moreover, no strand cuts are noticed (namely DNA form III is not present), in agreement with the electrophoresis data (Figure 12), which also suggest that **1**–**6** are not DNA cleavers. The AFM images obtained with compounds **3**, **5** and **6** are comparable (Figures 14e, 14g and 14h, respectively); some crossing points (green arrows) illustrating the possible initiation of supercoiling are noticed and supercoiled forms (white arrows) seem to be generated, especially for complex **5** (with visibly longer supercoiled forms; see white arrow in Figure 14g), which obviously exhibits the strongest interaction (compared to the other two compounds considered, namely **3** and **6**). With compound **1**, clearly a higher proportion of supercoiled forms of DNA are present (white arrows in Figure 14c). Furthermore, some early globular forms of DNA start to be seen (blue arrows in Figure 14); in fact, this feature is consistent with the electrophoretic results (Figure 12). Indeed, for complex **1**, at a concentration of 100 μM, the form I/form II bands are almost completely vanished (see corresponding lane 6 in Figure 12); actually, these bands are absent in lane 7. These microscopy data thus corroborate the proposed formation of large DNA-complex species at high concentrations of **1** (see above, section Gel electrophoresis). As a matter of fact, the AFM image obtained for complex **4** (Figure 14f) further confirms this proposal since only globular forms can be observed for this compound, which is the only one that does not show form I/form II bands at a complex concentration of 100 μM (see corresponding lane 6 in Figure 12). Finally, incubation of **2** with relaxed plasmid DNA clearly results in the almost complete disappearance of open circular structures (Figure 14d). The observed formation of supercoiled forms is indicative of a high affinity of the compound for the biomolecule. This AFM observation does not corroborate the corresponding gel-electrophoresis image (Figure 12, lane 6), where form II is still detected. However, without ascorbic acid (see Figure S15), the gel-electrophoresis result is in perfect agreement with that of AFM. Therefore, the presence of Form II in Figure 12 may be due to the presence of ascorbic acid (which appears to generate form II, see lanes 2 in Figure 12).

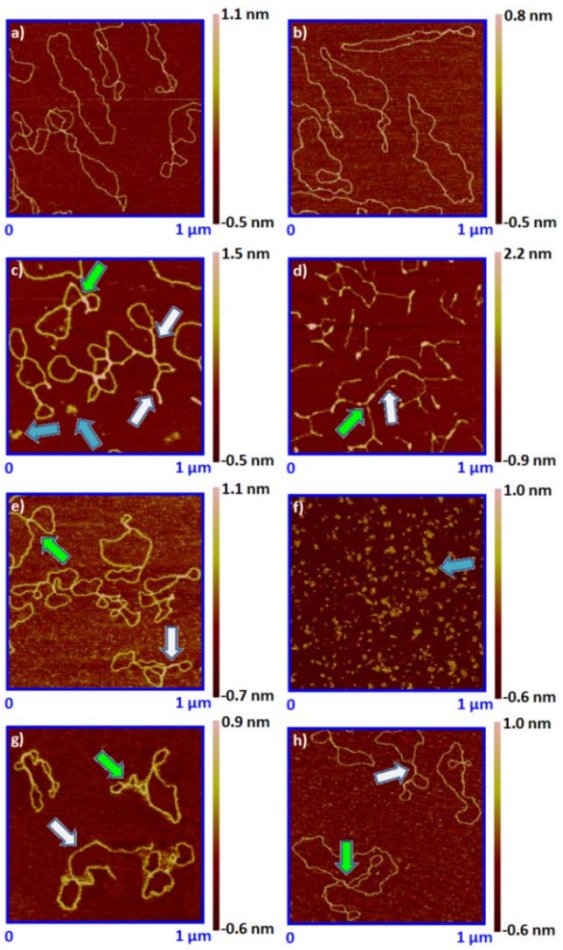

Fig. 14. AFM images of a) pure pBR322 plasmid DNA; b) plasmid DNA + ascorbic acid; c–h) plasmid DNA in the presence of complexes **1**–**6**, respectively. 200 ng DNA per sample; [complex] = 100 μM. The white arrows show supercoiling, the green arrows indicate crossing points, and the blue ones the initial formation of DNA globular aggregates.

Cytotoxicity assays: Although compounds **1–6** are not acting as DNA cleavers through the formation of ROS species (in contrast to the copper-pyrimol complex), their strong affinity for the double-stranded helix may make them good cytotoxic agents. Hence, cytotoxicity studies were carried out with three different murine cell lines (see Experimental Section). The IC_{50} values obtained for complexes **1**–**6** and cisplatin (as a reference) are listed in Table 4.

Table 4 IC_{50} values (μM) of copper complexes **1**–**6**, the ligands **HL1**–**HL4** and cisplatin against three murine cell lines, after 48 h of incubation. Data show means ± SD of three independent experiments.

Compound	L929[a]	S180[b]	EAT[c]
1	1.81 ± 0.23	2.05 ± 0.14	1.95 ± 0.06
2	2.39 ± 0.36	11.50 ± 4.84	2.68 ± 0.12
3	0.23 ± 0.01[d]	N.D[e]	0.24 ± 0.02[d]
4	5.22 ± 2.39[f]	0.27 ± 0.03[g]	1.11 ± 0.37[h]
5	- [i]	> 200	- [i]
6	1.57 ± 0.21[j]	26.93 ± 5.45[k]	2.57 ± 0.21[l]
HL1	2.87 ± 0.30	16.50 ± 3.63	142.70 ± 4.65
HL2	5.79 ± 2.07	69.27 ± 3.59	59.28 ± 5.97
HL3	0.04 ± 0.01	2.27 ± 0.27	38.72 ± 4.44
HL4	0.66 ± 0.4	1.20 ± 0.34	16.64 ± 3.36
cisplatin	29.05 ± 1.88	69.83 ± 0.17	60.13 ± 6.94

[a] Mouse fibroblasts; [b] Mouse sarcoma cells; [c] Ehrlich ascites tumour cells; [d] 0.46 μM based on Cu; [e] Not determined; [f] 10.44 μM based on Cu; [g] 0.54 μM based on Cu; [h] 2.22 μM based on Cu; [i] Too high value; [j] 4.71 μM based on Cu; [k] 80.79 μM based on Cu; [l] 7.71 μM based on Cu.

All compounds except complex **5** display very good cytotoxic properties with the three cell lines investigated, in all cases significantly better than cisplatin. The low cytotoxicity behaviour of **5**, which is the voluminous bis-cubane complex (Figure 5), may be due to its size (even as a monocubane in solution). Even though **5** shows high affinity for DNA, its bulkiness may prevent cellular internalization. Compounds **3** and **4**, *i.e.* the dinuclear complexes (Figures 3 and 4), present the greatest cytotoxic efficiencies, with submicromolar IC_{50} values that are about ten times smaller than those of the corresponding mononuclear complexes **1** and **2** (Table 4). Finally, compound **6**, which diverges from the series **1**–**5** because it contains modified **HL2'** ligands (Figure 6), behaves differently; **6** is active for two cell lines (L929 and EAT, with IC_{50} values in the range of those achieved with complexes **1** and **2**; Table 4), while it is less cytotoxic against mouse sarcoma cells (Table 4).

As mentioned in the introduction, the ligands **HL1**–**HL4** have been designed to bind biometals[13] such as copper. Therefore, the free ligands may also be used as potential cytotoxic agents; for instance, once inside the cell, such ligands may bind intracellular metal ions (like copper or zinc) and generate complexes that can lead to cell death. Actually, such a strategy has already been applied successfully. For example, elesclomol (N'^1,N'^3-dimethyl-N'^1,N'^3-di(phenylcarbonothioyl)malonohydrazide) is a potential novel anticancer agent (that has been evaluated in late-stage clinical trials),[72] whose apoptotic properties arise from its coordination to intracellular copper(II) ions that ultimately leads to generation of harmful reactive oxygen species (ROS).[73, 74]

Accordingly, cytotoxicity assays have been carried out with the free ligands as well. The four ligands are not significantly active against Ehrlich ascites tumour (EAT) cells, in contrast to the complexes (Table 4). For the mouse sarcoma (S180) cell line, the mononucleating ligands **HL1** and **HL2** are less active than the copper compounds; however, dinucleating **HL3** and **HL4** show good cytotoxic properties, with IC_{50} values in the range of that obtained with **1** (Table 4). Finally, for L929 fibroblasts, **HL1**–**HL4** present remarkable cytotoxicities, particularly **HL3** and **HL4** that give IC_{50} values of 0.04 μM (40 nM) and 0.66 μM, respectively (Table 4).

Conclusions

In the present study, a series of new Schiff-base ligands inspired by 4-methyl-2-*N*-(2-pyridylmethylene)aminophenol (Hpyrimol)[35] have been designed and synthesized. Taking into account the remarkable DNA-cleaving properties of the [Cu^{II}(pyrimol)Cl] complex,[33] copper coordination compounds from these Schiff-base ligands have been prepared and their DNA-interacting activities have been investigated using different characterization techniques. Unexpectedly, all copper complexes obtained are not capable of cleaving the DNA strands through a redox process, contrary to the copper/pyrimol moiety. However, all compounds strongly interact with DNA, most likely as groove binders. Actually, almost all of them show significant cytotoxicity properties, as evidenced by the submicromolar IC_{50} values achieved in some cases, with various cancer cell lines. Moreover, the free dinucleating ligands **HL3** and **HL4** (that can bind cellular metal ions) are also highly cytotoxic, especially against mouse fibroblasts with IC_{50} values in the nanomolar range.

The new family of highly cytotoxic copper coordination compounds obtained from Schiff-base ligands based on hydrazine derivatives display a drastically distinct mechanism of action compared to that of the original Cu/pyrimol complex. The mode of interaction of such complexes towards DNA is currently investigated thoroughly; for instance, the potential stabilization of G-quadruplexes by these planar (cationic) moieties is being examined. In addition, in vivo studies have been initiated with mice.

Experimental Section

Caution: Perchlorate salts are potentially explosive and should therefore be handled with extreme care.[75]

General methods

All reactions were performed under aerobic conditions and all reagents and solvents were purchased from Aldrich, Acros Organics or TCI Europe and were used as received. pBR322

DNA was purchased from Roche and *calf thymus* DNA was obtained from Sigma-Aldrich. ^{1}H spectra were recorded at room temperature with a Varian Unity 400 MHz spectrometer. Proton chemical shifts are expressed in parts per million (ppm, δ scale) and are referenced to the solvent peak. Infrared spectra (as KBr pellets) were recorded using a Nicolet-5700 FT-IR (in the range 4000–400 cm^{-1}), and data are represented as the frequency of absorption (cm^{-1}). Elemental analyses were performed by the Servei de Microanalisi, Consejo Superior de Investigaciones Cientifícas (CSIC) of Barcelona. The AFM images were obtained with a Multimode 8 AFM with electronic Nanoscope V scanning probe microscope from Bruker AXS, using the PEAK FORCE tapping mode. Commercial Si-tip on Nitride lever cantilevers (SNL, Bruker) with force constant of 0.4 N/m were used. The samples were deposited on mica disks (PELCO Mica Discs, 9.9 mm diameter; Ted Pella, Inc.), and dried before visualization. UV-Vis experiments were performed with a Varian Cary-100 spectrophotometer. The fluorescence measurements were carried out with a KONTRON SFM 25 spectrofluorometer. EPR spectra were recorded at 77 K with a Bruker ESP 300E X-band spectrometer coupled to a Bruker ER041 X-band frequency meter (9.45 GHz). The complexes were dissolved at room temperature in Tris-HCl/DMSO solvent mixtures (5 mM), and the solutions were frozen in liquid nitrogen. ESI Mass Spectroscopy was carried out using a LC/MSD-TOF Spectrometer from Agilent Technologies, equipped with an electrospray ionization (ESI) source at the Serveis Cientificotècnics of the Universitat de Barcelona.

General procedure for the preparation of the ligands

The ligands were synthesized by condensation reaction in refluxed methanol, between a hydrazinyl derivative (2-hydrazinopyridine or 2-hydrazinoquinoline, 10 mmol) and a monoaldehyde (3-*tert*-butyl-2-hydroxybenzaldehyde, 10 mmol; ligands **HL1** and **HL2**) or a dialdehyde (5-*tert*-butyl-2-hydroxyisophthalaldehyde, 5 mmol; ligands **HL3** and **HL4**). After a reaction time of four hours, the pure precipitated ligands were collected by filtration and dried under vacuum.

2-Tert-butyl-6-(pyridine-2-ylhydrazonomethyl)phenol ***(HL1)***: yield = 1.78 g (6.6 mmol, 66%). ^{1}H NMR ([D$_6$]DMSO): δ = 12.00 (s, OH), 11.48 (s, 1H), 8.23 (s, 1H), 8.19 (d, 1H, J = 8 Hz), 7.70 (t, 1H, J = 8 Hz), 7.19 (t, 2H, J = 8 Hz), 6.84 (m, 3H), 1.40 (s, 9 H) ppm; IR (KBr): $\bar{\upsilon}$ = 3452, 3200, 3047, 3000, 3000, 2869, 1950, 1700, 1600, 1578, 1439 cm^{-1}; elemental analysis calcd for $C_{16}H_{19}N_3O$ (269.35): C 71.35, H 7.11, N 15.60; found: C 71.66, H 7.22, N 15.64.

2-Tert-butyl-6-(quinoline-2-ylhydrazonomethyl)phenol ***(HL2)***: yield = 2.71 g (8.5 mmol, 85%). ^{1}H NMR ([D$_6$]DMSO): δ = 12.00 (s, OH), 11.48 (s, 1H), 8.31 (s, 1H), 8.82 (d, 1H, J = 8 Hz), 7.79 (d, 1H, J = 8 Hz), 7.63 (m, 3H), 7.30 (t, 1H, J = 8 Hz), 7.22 (d, 2H, J = 8 Hz), 7.18 (d, 1H, J = 8 Hz), 6.86 (t, 1H, J = 8 Hz), 1.43 (s, 9H) ppm; IR (KBr): $\bar{\upsilon}$ = 3439, 3334, 3047, 3004, 2947, 2665, 1950, 1700, 1600, 1508, 1430 cm^{-1}; elemental analysis calcd for $C_{20}H_{21}N_3O$ (319.41): C 75.21, H 6.63, N 13.16; found: C 75.13, H 6.71, N 13.14.

4-Tert-butyl-2,6-bis-(pyridine-2-ylhydrazonomethyl)phenol ***(HL3)***: yield = 1.77 g (4.6 mmol, 91%). ^{1}H NMR ([D$_6$]DMSO): δ = 12.00 (OH), 11.48 (s, 2H), 8.35 (s, 2H), 8.18 (d, 2H, J = 8 Hz), 7.68 (t, 2H, J = 8 Hz), 7.61 (s, 2H), 7.07 (d, 2H, J = 8 Hz), 6.79 (t, 2H, J = 8 Hz), 1.32 (s, 9H) ppm; IR (KBr): $\bar{\upsilon}$ = 3434, 3191, 3104, 2952, 2852, 1950, 1700, 1600, 1565, 1434 cm^{-1}; elemental analysis calcd for $C_{22}H_{24}N_6O$ (388.48): C 68.02, H 6.23, N 21.63; found: C 67.99, H 6.37, N 21.63.

4-Tert-butyl-2,6-bis-(quinoline-2-ylhydrazonomethyl)phenol ***(HL4)***: yield = 1.95 g (4.0 mmol, 80%). ^{1}H NMR ([D$_6$]DMSO): δ = 12.00 (s, OH), 11.48 (s, 2H), 8.47 (s, 1H), 8.20 (d, 1H, J = 8 Hz), 7.79 (d, 1H, J = 8 Hz), 7.60 (m, 3H), 7.43 (d, 1H, J = 8 Hz), 7.29 (t, 1H, J = 8 Hz), 1.35 (s, 9H) ppm; IR (KBr): $\bar{\upsilon}$ = 3421, 3203, 3042, 2951, 2846, 1950, 1700, 1613, 1504, 1434 cm^{-1}; elemental analysis calcd for $C_{30}H_{28}N_6O$ (488.60): C 73.75, H 5.78, N 17.20; found: C 73.65, H 5.72, N 16.84.

Preparation of coordination compounds 1–6

*Synthesis of [Cu(**L1**)Cl](CH$_3$OH) (**1**):* A methanolic solution (10 mL) of ligand **HL1** (100 mg, 0.37 mmol) was added to a methanolic solution (10 mL) of copper(II) chloride dihydrate (64 mg, 0.38 mmol). The resulting green reaction mixture was filtered and the filtrate was left unperturbed for the slow evaporation of the solvent. After one day, green single crystals (plates) of **1**, suitable for X-ray diffraction studies were obtained with a yield of 62% (92 mg, 0.23 mmol, based on **HL1**). IR (KBr): $\bar{\upsilon}$ = 3439, 3195, 3121, 3039, 2860, 1950, 1700, 1617 cm^{-1}; elemental analysis calcd for $C_{17}H_{22}ClCuN_3O_2$ (399.37): C 51.13, H 5.55, N 10.52; found: C 52.28, H 5.01, N 11.35.

*Synthesis of [Cu(**L2**)NO$_3$] (**2**)*: A methanolic solution (10 mL) of ligand **HL2** (100 mg, 0.31 mmol) was added to a methanolic solution (10 mL) of copper(II) nitrate trihydrate (75 mg, 0.31 mmol). The resulting green solution was filtered and the filtrate was left unperturbed for the slow evaporation of the solvent. After one day, green single crystals (lath crystals) of **2**, suitable for X-ray diffraction studies, were obtained with a yield of 44% (61 mg, 0.14 mmol, based on **HL2**). IR (KBr): $\bar{\upsilon}$ = 3386, 2956, 2865, 2782, 2413, 1950, 1700, 1621 cm^{-1}; elemental analysis calcd for $C_{20}H_{20}CuN_4O_4$ (443.95): C 54.14, H 4.54, N 12.62; found: C 53.88, H 4.62, N 12.33.

*Synthesis of [Cu$_2$(**L3**)(ClO$_4$)$_2$(CH$_3$O)(CH$_3$OH)](CH$_3$OH) (**3**)*: A methanolic (10 mL) solution of ligand **HL3** (119 mg, 0.31 mmol) was added to a methanolic solution (10 mL) of copper(II) perchlorate hexahydrate (238 mg, 0.64 mmol). The resulting green solution was filtered and the filtrate was left unperturbed for the slow evaporation of the solvent. After a few hours, small dark-green single crystals (prismatic crystals) of **3** were obtained with a yield of 71% (177 mg, 0.22 mmol, based on **HL3**). IR (KBr): $\bar{\upsilon}$ = 3404, 2965, 2865, 2765, 2421, 1950, 1700, 1630 cm^{-1}; elemental analysis calcd for $C_{25}H_{34}Cl_2Cu_2N_6O_{12}$ (808.58): C 37.14, H 4.24, N 10.39; found: C 36.70, H 4.12, N 10.20.

*Synthesis of [Cu$_2$(**L4**)(ClO$_4$)(OH)(CH$_3$OH)](ClO$_4$) (**4**)*: A methanolic solution (10 mL) of ligand **HL4** (102 mg, 0.21 mmol) was added to a methanolic solution (10 mL) of

copper(II) perchlorate hexahydrate (156 mg, 0.42 mmol). The resulting green solution was filtered and the filtrate was left unperturbed for the slow evaporation of the solvent. After a few hours, small dark-green single crystals (plates) of **4**, suitable for X-ray diffraction studies, were obtained with a yield of 63% (114 mg, 0.13 mmol, based on **HL4**). IR (KBr): $\bar{\upsilon}$ = 3439, 3217, 3060, 2960, 2600, 1950, 1700, 1626 cm^{-1}; elemental analysis calcd for ` (862.63): C 43.16, H 3.74, N 9.74; found: C 42.98, H 3.53, N 9.74.

Synthesis of $[Cu_8(\mathbf{L3})_4(NO_3)_4(OH)_5](NO_3)_3(CH_3OH)_5(H_2O)_8$ ***(5)***: A methanolic solution (10 mL) of ligand **HL3** (101 mg, 0.26 mmol) was added to a methanolic solution (10 mL) of copper(II) nitrate trihydrate (126 mg, 0.52 mmol). The resulting reaction mixture was filtered and the filtrate was left unperturbed for the slow evaporation of the solvent. After one day, green single crystals (prismatic crystals) of **5** were obtained with a yield of 53% (99 mg, 0.03 mmol, based on **HL3**). IR (KBr): $\bar{\upsilon}$ = 3452, 3226, 2952, 2865, 2352, 1950, 1700, 1617 cm^{-1}; elemental analysis calcd for [**5** – 3 CH_3OH + 7 H_2O], $C_{90}H_{127}Cu_8N_{31}O_{47}$ (2887.55): C 37.23, H 4.41, N 14.95; found: C 36.70, H 4.12, N 15.20.

Synthesis of $[Cu_3(\mathbf{HL2'})_4Cl_6](CH_3OH)_6$ ***(6)***: A methanolic solution (10 mL) of **HL2** (104 mg, 0.33 mmol) was added to a methanolic solution (10 mL) of copper(II) chloride dehydrate (42 mg, 0.25 mmol). The resulting green reaction mixture was filtered and the filtrate was left unperturbed for the slow evaporation of the solvent. After two days, green single crystals (block crystals) of **6**, suitable for X-ray diffraction studies, were obtained with a yield of 55% (84 mg, 0.045 mmol, based on **HL2**). IR (KBr): $\bar{\upsilon}$ = 3460, 3239, 3100, 2952, 2800, 1950, 1700, 1621 cm^{-1}; elemental analysis calcd for [**6** – 6 CH_3OH + 6 H_2O], $C_{80}H_{88}Cl_6Cu_3N_{12}O_{10}$ (1781.01.18): C 53.95, H 4.98, N 9.44; found: C 53.40, H 4.80, N 9.40.

X-ray crystallography

Data for compounds **1**, **2**, **4** and **6** were obtained at 100(2) K with a Bruker APEX II CCD diffractometer on the Advanced Light Source beamline 11.3.1 at Lawrence Berkeley National Laboratory, from a silicon 111 monochromater (λ = 0.7749 Å). Data for compounds **3** and **5** were recorded at 190(2) K on a Bruker APEX II equipped with a CCD area detector and a graphite monochromator (MoKα radiation λ = 0.71073 Å). Data reduction and absorption corrections were performed with SAINT and SADABS, respectively.[76] The structures were solved with SIR92 (**1, 2**, **4**, **6**)[77] and SIR97 (**3**, **5**),[78] and refined on F^2 with SHELXTL (**1, 2**, **4**, **6**) and SHELX97 (**3**, **5**).[79, 80] The PLATON SQUEEZE procedure[81] was used for compound **5** to treat regions of diffuse solvent which could not be sensibly modelled in terms of atomic sites. Their contribution to the diffraction pattern was removed and modified F_o^2 written to a new HKL file. The number of electrons thus located, 150 per unit cell, were included in the formula, formula weight, calculated density, μ and $F(000)$. This residual electron density was assigned to eight methanol molecules per unit cell. Crystallographic and refinement parameters are summarized in Tables S1 and S2. Selected bond distances and angles are given in Tables S3-S6. All details can be found in the supplementary crystallographic data for this paper in CIF format with CCDC numbers 964834–964839. These data can be obtained free of charge from The Cambridge Crystallographic Data Centre via www.ccdc.cam.ac.uk/data_request/cif

UV-Vis spectroscopy

The absorption titrations were achieved by adding increasing amounts (0–25 μM with 2.5 increments from 1 to 20 μM) of calf thymus DNA (ct-DNA) to complexes **1**–**6** (constant complex concentration of 25 μM) in Tris-HCl buffer (5 mM) and NaCl (50 mM) at pH = 7.2. The concentration of ct-DNA was determined from its absorption intensity at 260 nm with a molar extinction coefficient of 6600 M^{-1} cm^{-1}.[82] After addition of ct-DNA to the solution of metal complex, the resulting mixture was allowed to equilibrate at 25 °C for 10 min, after which the absorption spectra were recorded.

Fluorescence spectroscopy

Relative binding affinities of **1**–**6** to ct-DNA were investigated with EB-bound DNA (EB = ethidium bromide) in 5 mM Tris-HCl/50 mM NaCl buffer at pH = 7.2, containing 2% DMSO (DMSO was used to dissolve the copper(II) coordination compounds). The experiments were carried out at constant concentrations of ct-DNA and EB, respectively 2.5 and 12.5 μM, adding increasing amounts of the complex studied (from 2 to 150 μM). The EB concentration of 12.5 μM was determined by fluorescence spectroscopy through the addition of increasing amounts of EB to a 2.5 μM solution of ct-DNA, until a plateau was reached, which indicated the occupancy of all DNA-binding sites by the intercalator. The fluorescence spectra of all complexes were recorded at room temperature applying an excitation wavelength, λ_{exc}, of 514 nm. For the experiments with the minor-groove binder, a solution of Hoechst 33258 bound ct-DNA in 5 mM Tris–HCl/50 mM NaCl buffer (pH = 7.2) was used. The experiments were carried out at constant concentrations of ct-DNA and Hoechst 33258, respectively 0.19 and 15 μM, adding increasing amounts of the complex studied (from 2 to 150 μM). The fluorescence spectra were recorded at room temperature applying an excitation wavelength, λ_{exc}, of 350 nm.[83]

Gel electrophoresis experiments

Stock solutions of the copper(II) compounds were prepared in 40 mM HEPES/10 mM $MgCl_2$ buffer (pH = 7.2) containing 2% DMSO. pBR322 plasmid DNA aliquots (0.2 μg mL^{-1}) in 40 mM HEPES/10 mM $MgCl_2$ buffer were incubated with the complexes for 24 h at 37 °C. Subsequently, ascorbic acid (100 μM in 40 mM HEPES/10 mM $MgCl_2$ buffer) was added (in the case of the experiments without ascorbic acid, this step was not made) and the resulting mixture (containing 200 ng of DNA in a 100 μM solution of complex) was incubated at 37 °C for an additional hour. Next, the reaction samples were quenched with 4 μL of xylene and then electrophoretized on agarose gel (1% in TAE buffer, tris-acetate-EDTA) for 2 h at 1.5 V cm^{-1}, using a BIORAD horizontal tank connected to a PHARMACIA GPS

200/400 variable potential power supply. Samples of free DNA and DNA in presence of ascorbic acid were used as controls. Afterwards, the DNA was stained with SYBR® safe and the gel was photographed with a BIORAD Gel Doc™ EZ Imager.

Atomic-force microscopy experiments

pBR322 plasmid DNA was heated just before use at 60 °C for 10 min to obtain a homogeneous distribution of topoisomers. The stock solutions of the complexes and plasmid DNA, as well as the reaction samples (namely the DNA-complex-ascorbic acid mixtures) were prepared as above (see section Gel electrophoresis experiments). The AFM samples were prepared by casting a 2-μL drop of test solution onto freshly cleaved Muscovite green mica disks as the support. The drop was allowed to stand undisturbed for 3 min to favour the adsorbate/substrate interaction. Each DNA-laden disk was rinsed with Milli-Q water and was blown dry with clean compressed argon gas directed normal to the disk surface. The samples were stored over silica prior to AFM imaging.

Cell cultures

The murine breast cancer (Ehrlich ascites tumour; ATCC®# CCL-77™) and the murine sarcoma 180 tumour cells (S180; ATCC®# TIB-66 ™) were cultured in suspension in RPMI 1640 medium (pH 7.2 – 7.4) (Sigma Chemical Co., MO). The murine fibroblast normal cells (L929; ATCC®# CCL-1™) were cultured in DMEM medium (pH 7.2 – 7.4) (Sigma Chemical Co., MO). The cells were maintained humidified atmosphere (Thermo Scientfic) at 37 °C in 5% CO_2. Both media were supplemented with 10% fetal calf serum, 100 UI mL^{-1} penicillin G, 100 μg mL^{-1} streptomycin (all reagents were obtained from Gibco®, Invitrogen, Carlsbad, CA, USA).[84]

Cell-viability assays

The cytotoxic properties of all copper(II) coordination compounds investigated were evaluated applying the 3-(4,5-dimethylthiazol-2-yl)-2,5-diphenyl tetrazolium bromide (MTT) assay.[85] Thus, 1×10^5 S180 and EAT and 2×10^4 L929 cells were plated in 96-well tissue culture plates and subsequently treated with different concentrations of the copper (II) compounds (in the range 0.2-200 μM) for 48 h. After treatment, 10 μL MTT (5 mg mL^{-1}) (Sigma-Aldrich, St. Louis, MO, USA) were added to each well and the plates were incubated at 37 °C for another 3 h. The purple formazan crystals were dissolved in 50 μL SDS and the plates were kept in the dark overnight. Absorbance was determined at 545 nm using a Stat Fax 2100 microplate reader (Awareness Technology, Palm City, FL, USA). The cell viability was calculated as follows: Viability (%) = [(Absorbance of the treated wells) / (Absorbance of the control wells)] × 100. The IC_{50} values (which correspond to the compound concentrations, in μM that produce 50 % cell-viability reduction) were obtained from the dose-response curves using GraphPad Prism 4.02 for Windows (GraphPad Software, San Diego, CA, USA).

Acknowledgements

PG acknowledges ICREA (Institució Catalana de Recerca i Estudis Avançats) and the Ministerio de Economía y Competitividad (MINECO) of Spain (Project CTQ2011-27929-C02-01). The support of COST Action CM1105 is kindly acknowledged. The Advanced Light Source is supported by the Director, Office of Science, Office of Basic Energy Sciences of the U. S. Department of Energy under contract no. DE-AC02-05CH11231. OR acknowledges the Ministerio de Economía y Competitividad of Spain (Project MAT2011-24284).

Notes and references

[a] Departament de Química Inorgànica, Universitat de Barcelona, Martí i Franquès 1-11, 08028 Barcelona, Spain.
E-mail: patrick.gamez@qi.ub.es; Fax: +34 934907725 ; Homepage: www.bio-inorganic-chemistry-icrea-ub.com
[b] Laboratório de Genética Molecular e Citogenética, Instituto de Ciências Biológicas, Universidade Federal de Goiás, UFG, Goiânia, Goiás, Brazil.
E-mail: silveiralacerda@gmail.com
[c] Dipartimento di Chimica, Università degli Studi di Parma, Vialle delle Scienze 17/A, 43124 Parma, Italy.
[d] Instituto de Ciencia de Materiales de Aragón (ICMA), CSIC and Universidad de Zaragoza, Plaza San Francisco s/n, 50009 Zaragoza, Spain.
[e] Advanced Light Source (ALS), Lawrence Berkeley National Laboratory, 1 Cyclotron Road, Berkeley CA 94720, USA.
[f] Institució Catalana de Recerca i Estudis Avançats (ICREA), Passeig Lluís Companys 23, 08010 Barcelona, Spain.

† Electronic Supplementary Information (ESI) available: Crystal data and structure refinement for **1**–**6**; illustrations of the crystal packing of **1**, **2**, **4** and **6**; selected bond lengths and angles for **1**–**6**; absorption spectra for **2**–**6** in the presence of DNA; ESI-MS spectra for **1**–**6**; EPR spectra; fluorescence spectra of the complex EB-DNA in the presence of **2**–**6** and agarose gel electrophoresis experiments without reducing agent. See DOI: 10.1039/b000000x/

1. Komeda, S.; Casini, A., *Curr. Top. Med. Chem.* **2012,** *12*, 219-235.
2. Liu, H. K.; Sadler, P. J., *Acc. Chem. Res.* **2011,** *44*, 349-359.
3. Bruijnincx, P. C. A.; Sadler, P. J., *Curr. Opin. Chem. Biol.* **2008,** *12*, 197-206.
4. Paterson, B. M.; Donnelly, P. S., *Chem. Soc. Rev.* **2011,** *40*, 3005-3018.
5. Brabec, V.; Novakova, O., *Drug Resist. Update* **2006,** *9*, 111-122.
6. Rosenberg, B.; van Camp, L.; Grimley, E. B.; Thomson, A. J., *J. Biol. Chem.* **1967,** *242*, 1347-1352.
7. Thomson, A. J., The Discovery, Use and Impact of Platinum Salts as Chemotherapy Agents for Cancer. In Christie, D. A.; Tansey, E. M., Eds. Wellcome Witnesses to Twentieth Century Medicine: London: Wellcome Trust Centre for the History of Medicine at UCL, 2007; Vol. 30.
8. Zhang, C. X.; Lippard, S. J., *Curr. Opin. Chem. Biol.* **2003,** *7*, 481-489.
9. Wang, D.; Lippard, S. J., *Nat. Rev. Drug Discov.* **2005,** *4*, 307-320.
10. Reedijk, J., *Eur. J. Inorg. Chem.* **2009**, 1303-1312.
11. Kelland, L. R., *Drugs* **2000,** *59*, 1-8.

12. *Bioinorganic Medicinal Chemistry*. Wiley-VCH: Weinheim, 2011.
13. Pfaender, S.; Grabrucker, A. M., *Metallomics* **2014,** *6*, 960-977.
14. Linder, M. C., *Biochemistry of Copper*. Plenum Press: New York, 1991.
15. Harris, E. D., *Nutr. Rev.* **2001,** *59*, 281-285.
16. Lippard, S. J.; Berg, J. M., *Principles of bioinorganic chemistry*. University Science Books: Mill Valley, CA., 1994.
17. Halliwell, B.; Gutteridge, J. M. C., *Method Enzymol.* **1990,** *186*, 1-85.
18. Wang, T.; Guo, Z. J., *Curr. Med. Chem.* **2006,** *13*, 525-537.
19. Jomova, K.; Valko, M., *Toxicology* **2011,** *283*, 65-87.
20. Valko, M.; Rhodes, C. J.; Moncol, J.; Izakovic, M.; Mazur, M., *Chem.-Biol. Interact.* **2006,** *160*, 1-40.
21. Daniel, K. G.; Harbach, R. H.; Guida, W. C.; Dou, Q. P., *Front. Biosci.* **2004,** *9*, 2652-2662.
22. Garbutcheon-Singh, K. B.; Grant, M. P.; Harper, B. W.; Krause-Heuer, A. M.; Manohar, M.; Orkey, N.; Aldrich-Wright, J. R., *Curr. Top. Med. Chem.* **2011,** *11*, 521-542.
23. Duncan, C.; White, A. R., *Metallomics* **2012,** *4*, 127-138.
24. van Rijt, S. H.; Sadler, P. J., *Drug Discov. Today* **2009,** *14*, 1089-1097.
25. Norden, A. D.; Drappatz, J.; Wen, P. Y., *Lancet Neurol.* **2008,** *7*, 1152-1160.
26. Zeglis, B. M.; Pierre, V. C.; Barton, J. K., *Chem. Commun.* **2007**, 4565-4579.
27. Wu, L. S.; Reymer, A.; Persson, C.; Kazimierczuk, K.; Brown, T.; Lincoln, P.; Norden, B.; Billeter, M., *Chem.-Eur. J.* **2013,** *19*, 5401-5410.
28. Brissos, R. F.; Garcia, S.; Presa, A.; Gamez, P., *Comments Inorg. Chem.* **2011,** *32*, 219-245.
29. Maheswari, P. U.; van der Ster, M.; Smulders, S.; Barends, S.; van Wezel, G. P.; Massera, C.; Roy, S.; den Dulk, H.; Gamez, P.; Reedijk, J., *Inorg. Chem.* **2008,** *47*, 3719-3727.
30. de Hoog, P.; Louwerse, M. J.; Gamez, P.; Pitie, M.; Baerends, E. J.; Meunier, B.; Reedijk, J., *Eur. J. Inorg. Chem.* **2008**, 612-619.
31. Maheswari, P. U.; Barends, S.; Ozalp-Yaman, S.; de Hoog, P.; Casellas, H.; Teat, S. J.; Massera, C.; Lutz, M.; Spek, A. L.; van Wezel, G. P.; Gamez, P.; Reedijk, J., *Chem.-Eur. J.* **2007,** *13*, 5213-5222.
32. Maheswari, P. U.; Lappalainen, K.; Sfregola, M.; Barends, S.; Gamez, P.; Turpeinen, U.; Mutikainen, I.; van Wezel, G. P.; Reedijk, J., *Dalton Trans.* **2007**, 3676-3683.
33. Maheswari, P. U.; Roy, S.; den Dulk, H.; Barends, S.; van Wezel, G.; Kozlevcar, B.; Gamez, P.; Reedijk, J., *J. Am. Chem. Soc.* **2006,** *128*, 710-711.
34. Ozalp-Yaman, S.; de Hoog, P.; Maheswari, P. U.; Casellas, H.; Golobic, A.; Kozlevcar, B.; Gamez, P.; Reedijk, J., *Electrochim. Acta* **2010,** *55*, 8655-8663.
35. de Hoog, P.; Pachon, L. D.; Gamez, P.; Lutz, M.; Spek, A. L.; Reedijk, J., *Dalton Trans.* **2004**, 2614-2615.
36. Jazdzewski, B. A.; Tolman, W. B., *Coord. Chem. Rev.* **2000,** *200*, 633-685.
37. Li, W.; Zhang, Z. W.; Wang, S. X.; Ren, S. M.; Jiang, T., *Chem. Biol. Drug Des.* **2009,** *74*, 80-86.
38. Zhao, J. Y.; Li, W.; Ma, R.; Chen, S. P.; Ren, S. M.; Jiang, T., *Int. J. Mol. Sci.* **2013,** *14*, 16851-16865.
39. Sartorius, J.; Schneider, H. J., *J. Chem. Soc.-Perkin Trans. 2* **1997**, 2319-2327.
40. Koval, I. A.; Gamez, P.; Belle, C.; Selmeczi, K.; Reedijk, J., *Chem. Soc. Rev.* **2006,** *35*, 814-840.
41. Rolff, M.; Schottenheim, J.; Decker, H.; Tuczek, F., *Chem. Soc. Rev.* **2011,** *40*, 4077-4098.
42. Das, S.; Pal, S., *Inorg. Chim. Acta* **2010,** *363*, 3028-3035.
43. Addison, A. W.; Rao, T. N.; Reedijk, J.; Vanrijn, J.; Verschoor, G. C., *J. Chem. Soc.-Dalton Trans.* **1984**, 1349-1356.
44. Sadana, A. K.; Mirza, Y.; Aneja, K. R.; Prakash, O., *Eur. J. Med. Chem.* **2003,** *38*, 533-536.
45. Kumar, D.; Sekhar, K.; Dhillon, H.; Rao, V. S.; Varma, R. S., *Green Chem.* **2004,** *6*, 156-157.
46. Gibson, M. S., *Tetrahedron* **1963,** *19*, 1587-1589.
47. Pollak, A.; Tisler, M., *Tetrahedron* **1966,** *22*, 2073-2079.
48. Bourgeois, P.; Cantegril, R.; Chene, A.; Gelin, J.; Mortier, J.; Moyroud, J., *Synth. Commun.* **1993,** *23*, 3195-3199.
49. Ciesielski, M.; Pufky, D.; Doring, M., *Tetrahedron* **2005,** *61*, 5942-5947.
50. Shahabadi, N.; Fatahi, P., *DNA Cell Biol.* **2012,** *31*, 1328-1334.
51. Long, E. C.; Barton, J. K., *Acc. Chem. Res.* **1990,** *23*, 271-273.
52. Asadi, M.; Safaei, E.; Ranjbar, B.; Hasani, L., *New J. Chem.* **2004,** *28*, 1227-1234.
53. Bradley, P. M.; Angeles-Boza, A. M.; Dunbar, K. R.; Turro, C., *Inorg. Chem.* **2004,** *43*, 2450-2452.
54. Inclan, M.; Albelda, M. T.; Frias, J. C.; Blasco, S.; Verdejo, B.; Serena, C.; Salat-Canela, C.; Diaz, M. L.; Garcia-Espana, A.; Garcia-Espana, E., *J. Am. Chem. Soc.* **2012,** *134*, 9644-9656.
55. Bhat, S. S.; Kumbhar, A. S.; Kumbhar, A. A.; Khan, A., *Chem.-Eur. J.* **2012,** *18*, 16383-16392.
56. Kashanian, S.; Javanmardi, S.; Chitsazan, A.; Omidfar, K.; Paknejad, M., *DNA Cell Biol.* **2012,** *31*, 1349-1355.
57. Norden, B.; Tjerneld, F.; Palm, E., *Biophys. Chem.* **1978,** *8*, 1-15.
58. Loontiens, F. G.; McLaughlin, L. W.; Diekmann, S.; Clegg, R. M., *Biochemistry* **1991,** *30*, 182-189.
59. Loontiens, F. G.; Regenfuss, P.; Zechel, A.; Dumortier, L.; Clegg, R. M., *Biochemistry* **1990,** *29*, 9029-9039.
60. Healy, E. F., *J. Chem. Educ.* **2007,** *84*, 1304-1307.
61. Knapp, S.; Keenan, T. P.; Zhang, X. H.; Fikar, R.; Potenza, J. A.; Schugar, H. J., *J. Am. Chem. Soc.* **1990,** *112*, 3452-3464.
62. Suresh, E.; Bhadbhade, M. M.; Srinivas, D., *Polyhedron* **1996,** *15*, 4133-4144.
63. Lepecq, J. B.; Paoletti, C., *J. Mol. Biol.* **1967,** *27*, 87-106.
64. Meyer-Almes, F. J.; Porschke, D., *Biochemistry* **1993,** *32*, 4246-4253.
65. Lepecq, J. B.; Nguyendanghung; Gosse, C.; Paoletti, C., *Proc. Natl. Acad. Sci. U. S. A.* **1974,** *71*, 5078-5082.
66. Dehkordi, M. N.; Lincoln, P., *J. Fluoresc.* **2013,** *23*, 813-821.
67. Peberdy, J. C.; Malina, J.; Khalid, S.; Hannon, M. J.; Rodger, A., *J. Inorg. Biochem.* **2007,** *101*, 1937-1945.
68. McCoubrey, A.; Latham, H. C.; Cook, P. R.; Rodger, A.; Lowe, G., *FEBS Lett.* **1996,** *380*, 73-78.
69. Cosa, G.; Focsaneanu, K. S.; McLean, J. R. N.; McNamee, J. P.; Scaiano, J. C., *Photochem. Photobiol.* **2001,** *73*, 585-599.
70. Escribano, E.; Font-Bardia, M.; Calvet, T.; Lorenzo, J.; Gamez, P.; Moreno, V., *Inorg. Chim. Acta* **2013,** *394*, 65-76.
71. Gamba, I.; Salvado, I.; Rama, G.; Bertazzon, M.; Sanchez, M. I.; Sanchez-Pedregal, V. M.; Martinez-Costas, J.; Brissos, R. F.; Gamez, P.;

Mascarenas, J. L.; Lopez, M. V.; Vazquez, M. E., *Chem. Eur. J.* **2013,** *19*, 13369-13375.
72. Vo, N. H.; Xia, Z. Q.; Hanko, J.; Yun, T.; Bloom, S.; Shen, J. H.; Koya, K.; Sun, L. J.; Chen, S. J., *J. Inorg. Biochem.* **2014,** *130*, 69-73.
73. Nagai, M.; Vo, N. H.; Ogawa, L. S.; Chimmanamada, D.; Inoue, T.; Chu, J.; Beaudette-Zlatanova, B. C.; Lu, R. Z.; Blackman, R. K.; Barsoum, J.; Koya, K.; Wada, Y., *Free Radic. Biol. Med.* **2012,** *52*, 2142-2150.
74. Kirshner, J. R.; He, S. Q.; Balasubramanyam, V.; Kepros, J.; Yang, C. Y.; Zhang, M.; Du, Z. J.; Barsoum, J.; Bertin, J., *Mol. Cancer Ther.* **2008,** *7*, 2319-2327.
75. Zettler, M. W., *Iron(II) Perchlorate* e-EROS: Electronic Encyclopedia of Reagent for Organic Synthesis, Wiley-VCH: 2001.
76. *SAINT and SADABS*, Bruker AXS Inc.: Madison, Wisconsin, USA.
77. Altomare, A.; Cascarano, G.; Giacovazzo, C.; Guagliardi, A., *J. Appl. Crystallogr.* **1993,** *26*, 343-350.
78. Altomare, A.; Burla, M. C.; Camalli, M.; Cascarano, G. L.; Giacovazzo, C.; Guagliardi, A.; Moliterni, A. G. G.; Polidori, G.; Spagna, R., *J. Appl. Crystallogr.* **1999,** *32*, 115-119.
79. Sheldrick, G. M. *SHELXTL*, Bruker AXS Inc.: Madison, Wisconsin, USA.
80. Sheldrick, G. M., *Acta Crystallogr. Sect. A* **2008,** *64*, 112-122.
81. van der Sluis, P.; Spek, A. L., *Acta Crystallogr. Sect. A* **1990,** *46*, 194-201.
82. Marmur, J., *J. Mol. Biol.* **1961,** *3*, 208-218.
83. Matsuba, Y.; Edatsugi, H.; Mita, I.; Matsunaga, A.; Nakanishi, O., *Cancer Chemother. Pharmacol.* **2000,** *46*, 1-9.
84. Menezes, C. S. R.; Costa, L.; Avila, V. D.; Ferreira, M. J.; Vieira, C. U.; Pavanin, L. A.; Homsi-Brandeburgo, M. I.; Hamaguchi, A.; Silveira-Lacerda, E. D., *Chem.-Biol. Interact.* **2007,** *167*, 116-124.
85. Mosmann, T., *J. Immunol. Methods* **1983,** *65*, 55-63.

Graphical Abstract

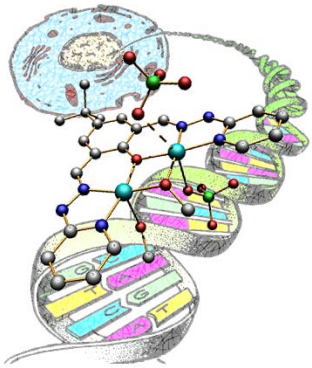

Copper complexes from Schiff-base ligands show high cytotoxicity against diverse cancer cell lines, with IC_{50} values down to 0.23 μM.